B.A.R.C.-608

B.A.R.C.-608

सत्यमेव जयते

GOVERNMENT OF INDIA
ATOMIC ENERGY COMMISSION

VAN DE GRAAFF LABORATORY PROGRESS REPORT

Compiled by

T. P. David
Nuclear Physics Division

BHABHA ATOMIC RESEARCH CENTRE
BOMBAY, INDIA
1972

B. A. R. C. -608

GOVERNMENT OF INDIA
ATOMIC ENERGY COMMISSION

B. A. R. C. -608

VAN DE GRAAFF LABORATORY PROGRESS REPORT

Compiled by

T. P. David
Nuclear Physics Division

BHABHA ATOMIC RESEARCH CENTRE
BOMBAY, INDIA
1972

CONTENTS

INTRODUCTION

This report summarises the operation and utilization of the accelerator during the year 1971. The 5.5 MeV Van de Graaff accelerator has completed its 10th year of operation. From the end of 1964 the machine has been operated on a round-the-clock 7 day week schedule.

The import requirement for the running and maintenance of the machine has been brought to a minimum by fabricating most of the components in the laboratory and by utilizing locally available substitutes with modifications wherever necessary. Equipment for the beam transport used with the accelerator such as the five-port beam switching magnet, quadrupole focuseing lenses, beam deflectors and power supplies are all fabricated in the laboratory and these are giving satisfactory service.

The 400 kV Van de Graaff machine has been used during the year mostly for ion implantation studies.

A number of research experiments have been carried out with the accelerator during the period under review and brief accounts of this work are summarised in this report.

Accelerator operation

I. Analysis of Machine Operation

Machine run

Total time available from 1st January 1971 to 31st December 1971	..	8760 Hours
Holiday observed during the year	..	48 "
Time lost due to chiller and Airconditioning plant failures	..	744 "
Time used for routine maintenance	..	288 "
Time lost due to power failure	..	24 "
Time lost due to water supply failure	..	6 "
Time lost due to nonavailability of Liquid nitrogen	..	720 "
Time utilized for installation of He^{++} system	..	408 "
Time lost due to breakdowns	..	1744* "
Total time machine run	..	4778 "

Machine utilization

Time used for research experiments	..	3631 Hours
Experimental time lost due to machine conditioning, beam alignment and failure of beam transport equipment and vacuum systems	..	1147 Hours
		4778 Hours

---

* Of this 392 hours have been used in transferring insulating gas and pumping out air from the accelerator tank.

II. Modifications and additions to the accelerator

1. A new stream-lined compact gas manifold has been designed, fabricated and installed in the accelerator terminal. This has considerably reduced the possibility of pressure leaks and has made easy the replacement of thermo-mechanical leaks.

2. Two additional fans have been installed on the accelerator control console for cooling the power supplies and electronic units.

3. The oil cooled 8 amp. variac assembly in the 5-port switching magnet power supply has been replaced by a 15 amp. 3 phase variac. The variac is remote controlled motor operated and provided with limit switches. This has been necessary to ensure trouble free operation of this supply when working with high currents over long periods of time.

4. A stabilized transistorised power supply has been provided for the quadrupole magnets used in the beam tube. This unit was built and supplied by the research group from the Tata Institute of Fundamental Research, Bombay.

5. A versatile leak test assembly using a 10 cm diffusion pump has been built and commissioned for use with accelerator components fabrication and test work.

6. A new solenoid operated water-cooled beam stopper assembly has been fabricated and installed replacing the old unit which was giving frequent trouble due to water leaks into the stopper chamber.

III. Linearity test on the Analyzing Magnet

An attempt was made to determine the saturation effect and nonlinearity of the beam analyzing magnet in July 1971. For the test, the magnetic field at the centre of the pole face close to the analyzing chamber was measured by noting the NMR resonance frequency while the magnet current was determined by an electrometer voltmeter unit monitoring the voltage across the standard resistance in series with the magnet coil.

It was noted that nonlinearity starts from approximately a magnetic field corresponding to 4 MeV $^4He^+$ beam energy. Also it was observed that the magnetic fields measured at points away from the centre do not follow variations corresponding to that at the centre. Details are published elsewhere in this report.

IV. Major breakdowns

1. Belt charge system was found defective. The fault was traced to an overheated transformer in the current control unit. This transformer has been since rewound in the laboratory and tested.
2. The water cooling coil in the solenoid operated beam stopper unit developed leak. The defect was initially rectified by using araldite at the leak point. A new beam stopper assembly has been since fabricated and the defective unit has been replaced.
3. The beam transmission through the 5-port switching chamber was found unsatisfactory. This was caused by poor vacuum in the chamber due to the development of a small hole on the chamber wall. The chamber was removed and the hole was sealed by welding and tested.

4. A micro-leak of insulating gas into the accelerator tube was noticed during the middle of September when the tank was being pressurised. The leak was located in a coupling on the gas manifold. However, since the leak was apparent only at very high tank pressures, 9 days of machine time was lost before it could be located and rectified.

5. The accelerator could not be run for about a month due to defect in the air-conditioning and chilled water supply plants. Another month of machine time was lost due to short supply of liquid nitrogen essential for maintaining good vacuum in the system. This period was utilized for carrying out major maintenance work on the accelerator such as overhauling of vacuum systems and other auxiliary equipments, carrying out performance tests on all electronic and control units and fabrication of replacement accelerator components.

V. Terminal modifications for the production of doubly ionized Helium beam

The results of the bench test on the cross field analyzer system* for separating pre-focussed doubly charged helium ions have been very satisfactory. Modification of the accelerator terminal for installing this system was started by the middle of December 1971. To provide space for the source bottle and separation assembly the high voltage dome was raised by about 7.5 cms by installing a stainless steel collar between the dome and the top of the column assembly. Additional units such as 5 kV probe voltage supply, 35 kV Einzel lens prefocus supply, magnet power and deflector voltage supplies and the 100 W RF oscillator and its power supply were accommodated on the terminal. The additional control variacs were fixed on the terminal and their reversible motor

*S.N. Misra and M.R. Dwarkanath, B.A.R.C./I-120 (1971) drives were installed on the tank base. The assembly is undergoing operational tests. When brought into operation this will provide higher currents of the various charged particle beams as well as 11 MeV doubly charged helium ion beam.

VI. PN 400 Van de Graaff Machine

This machine has been used for 359 hours during the period under report mostly for ion implantation studies. The terminal of the accelerator has been modified to accommodate two gas bottles with remote controls enabling changing over from one gas to another while the machine is under operation. A beam deflector with two pairs of deflector plates perpendicular to each other has been installed in the beam tube. One square centimetre target area can now be uniformly scanned by the ion beam by applying saw tooth voltage at different frequencies to these plates. Details are given else where in this report.

A 90° analyzing magnet to be fabricated with low carbon Tata 'A' grade steel has been designed. The design drawings have been completed and the magnet is under fabrication at the B.A.R.C. Central Workshop. The magnet coil is designed to be wound from extruded aluminium tubing of 12.7 mm side square section through which the cooling water is circulated to achieve maximum cooling efficiency. The stabilized transistorised power supply for the magnet will have a maximum rating of 250 Amps at 15 V output.

RESEARCH EXPERIMENTS

1. A Study of the Reaction $^{64}Ni(p,p)^{64}Ni$ In the Range 3.150 to 4.025 MeV - S.K. Gupta, S.S. Kerekatte, M.K. Mehta and A.S. Divatia - The present work is an extension of experimental programme for the study of levels in ^{65}Cu. The first part of this programme was the previously reported work[1)] on the $^{64}Ni(p,n)^{64}Cu$ reaction. We have studied the elastic scattering of protons from ^{64}Ni to investigate the isobaric analogue resonances in the nucleus ^{65}Cu corresponding to the parent nucleus ^{65}Ni. This reaction has also been studied by the Duke group[2)] from Ep = 2.5 - 3.3 MeV. In the energy range Ep = 3.150 - 4.025 MeV scanned by us, resonances have been observed which are superimposed on a large amount of fine structure.

A ^{64}Ni target (enriched to 97.92%) was prepared by evaporating ^{64}Ni metal from a heated tungsten ribbon on to a thin carbon film. The target thickness was estimated to be 1 keV for 4.0 MeV protons. Four solid state detectors at laboratory angles of 89°, 124.5°, 140° and 165° were used to detect the scattered protons. The first three angles correspond to the zeroes of Legendre polynomials of first, second and third orders. Around the energies where strong anomalies were observed, data were taken in 2.5 keV steps and elsewhere in 5 keV steps. The whole excitation function is shown in Fig. 1. The 1 keV steps data are shown in Fig. 2

Strong anomalies have been observed at E_{plab} = 3.220 and 3.873 MeV. These correspond to the parent states at 0.065 (first excited state) and 0.615 MeV (third excited state) in ^{65}Ni as observed in the $^{64}Ni(d,p)^{65}Ni$ reaction[3]. As observed in the (d,p) reaction they should have $l_p = 1$. There should be a resonance around 3.48 MeV corresponding to the parent state in ^{65}Ni at 0.315 MeV (second excited state). No anomaly could be found around this energy in the 5 keV steps data. Measurements were made with 1 keV step from 3.475 to 3.510 MeV. As shown in fig. 2 the anomaly was observed in this region. However, the (d,p) data assigns a value of $l_n = 1$ to this state. But in that case the anomaly should be very weak at 90° relative to the other angles. This is not the case as observed here. It may indicate that $l_p = 0$ for the corresponding state. The shape analysis of these resonances will be carried out and the data will be extended to higher energies where the (p,n) reaction also shows strong resonance effects.

The results are displayed in Table I.

Table I

Levels in ^{65}Ni (ref.3)			Resonances in ^{65}Cu (present work)		
E_x (MeV)	l_n	$(2J+1)S$	$E_p^{c.m}$ (MeV)	l_p	coulomb displacement energy (MeV)
0.065	1	1.23	3.170	1	9.207
0.315	1	0.173	3.441	0	9.228
0.699	1	0.615	3.813	1	9.216

1) S.S. Kerekatte, S.K. Gupta and A.S. Divatia, Proc. of Nucl. Phys. and Solid State Phys. Symposium, India (1970)45

2) J.C. Browne, H.W. Newson, E.G. Bilpuch and G.E. Mitchell, Nucl. Phys. A153(1970)481

3) R.H. Fulmer and A.L. McCarthy, Phys. Rev. 131(1963)2133

2. Studies on Analog States in ^{33}Cl by Isospin-Forbidden Resonances in the Reaction $^{32}S(p,\gamma)^{33}Cl$* - M.A. Eswaran, M. Ismail, N.L. Ragoowansi and H.H. Oza - The residual activity between bursts of a mechanically chopped beam has been used to measure the yield of the reaction $^{32}S(p,\gamma)^{33}Cl$ systematically in the bombarding energy range E_p = 3.36 to 5.41 MeV. Two, T = 3/2 states in ^{33}Cl at E_p = 3.371 ± 0.005 MeV, E_x = 5.550 ± 0.007 MeV and at E_p = 5.282 ± 0.006 MeV E_x = 7.402 ± 0.008 MeV have been located with the resonance strengths $(2J+1)\Gamma_{p_0}\Gamma_\gamma/\Gamma$ = 0.76 ± 0.18 eV and 1.50 ± 0.37 eV respectively. Each of these resonances was narrower than the estimated 2 keV spread in the proton beam. These two states are interpreted as the analogs of the ground and the second excited state of ^{33}P with J^π values, $1/2^+$ and $5/2^+$ respectively. γ-decay of the lower resonance, investigated with a Ge(Li) detector shows > 88% and < 12% branchings to the first excited state and ground state of ^{33}Cl respectively. The M1 strengths of these transitions are compared with those obtained from beta analog transitions and with the theoretical predictions based on the many-particle shell model calculations.

3. Elastic Scattering of Protons on ^{66}Zn - M.G. Betigeri, C.M. Lamba, D.K. Sood, N. Sarma and N.S. Thampi - We have completed the study of the resonances in the compound nucleus ^{67}Ga which are isobaric analogue states of 184, 363, 978 and 1142 keV levels of ^{67}Zn. The analogue of ^{67}Zn ground state ($5/2^-$) could not be observed because of the high value of the angular momentum involved. No significant anamoly for 93 keV analogue could be observed. Shapes of all the resonances indicate the transferred angular momentum to be ℓ = 1.

---

*To be published in Physical Review C (1972)

The assignment of 978 keV level in ^{67}Zn as being populated by ℓ = 2 in the study of the reaction $^{66}Zn(d,p)^{67}Zn$ seems to be erroneous. The shapes of the resonances at three angles were analysed using the computer programme ANSPEC. The excitation functions are shown in Fig. 3 and the fits to the various resonances are shown in fig 4(a,b,c) . Following set of optical potential was used.

$$V = 50.5 \text{ MeV}$$
$$W = 13.5 \text{ MeV}$$
$$r_{or} = 1.25 \text{ f} \qquad a_{or} = .65 \text{ f}$$
$$r_{oi} = 1.25 \text{ f} \qquad a_{oi} = .47 \text{ f}$$
$$r_{oc} = 1.3 \text{ f}$$

The analysis yields values of Γp for the isobaric analogue states which is related to the spectroscopic factor for the corresponding transition in $^{66}Zn(d,p)^{67}Zn$ reaction. The values of spectroscopic factors (S_{pp}) so extracted compare well with the values S_{dp} obtained from (d,p) reaction. The relevent results are listed in Table 2 .

4. <u>Analogue States in ^{73}As via the $^{72}Ge(p,p'e)$ Reaction</u> - M.G. Betigeri, C.M. Lamba, D.K. Sood and N.S. Thampi - The low lying states of ^{73}Ge have been excited as isobaric analogue states in ^{73}As by the proton bombardment of ^{72}Ge. The decay of these states in the inelastic channel (0^+, 690 keV in ^{72}Ge) are observed by detecting the internal conversion electrons using the β -spectrometer. The reaction is studied in the energy range of Ep = 3.315 MeV to 4.7 MeV. Total cross section is measured as a function of energy. From the proper identification of analogue states, we have deduced the values of Γp , $\Gamma p'$ and Γ . On the basis of these results the level at 67 and 673 keV in ^{73}Ge are interpreted to be single particle neutron states

Table 2

E_p	E_{exc} in ^{67}Ga(MeV)	Energies of levels in ^{67}Zn (present)	^{66}Zn(d,p)	ℓ	Γ	Γ_p	S_{pp}	S_{dp}
3.021	8.294	184	184	1	4	0.1	0.07	0.08
3.814	9.087	978	980	1	5.00	1.00	0.12	-
3.978	9.251	1142	1142	1	10.0	2.0	0.21	0.37

Table 3

E (keV)	α_K expt.	α_K Theory E3	M1	E2	Multipolarity
130	1.9 ± 0.1	1.9	-	-	E3
218	(2.6 ± 0.3) × 10^{-2}	-	1.4 × 10^{-2}	4.6 × 10^{-2}	(E2 + M1)
260	(1.9 ± 0.1) × 10^{-2}	-	0.9 × 10^{-2}	2.5 × 10^{-2}	(M1 + E2)
275	(7.4 ± 0.2) × 10^{-3}	-	7.8 × 10^{-3}	2.0 × 10^{-2}	M1
302	(1.7 ± 0.2) × 10^{-2}	-	6.0 × 10^{-3}	1.5 × 10^{-2}	E2
383	(3.2 ± 0.2) × 10^{-3}	-	3.4 × 10^{-3}	6.6 × 10^{-3}	M1
401	(6.0 ± 0.4) × 10^{-3}	-	3.1 × 10^{-3}	5.8 × 10^{-3}	E2
445	(2.8 ± 0.3) × 10^{-3}	-	2.5 × 10^{-3}	4.2 × 10^{-3}	M1

built on the second 0^+ in ^{72}Ge.

(To be published in Nuclear Physics)

5. <u>Conversion electron Studies following $^{80}Se(p,n)^{80}Br$, $^{79,81}Br(p,n)^{79,81}Kr$ reactions</u> - Y.K. Agarwal*, C.V.K. Baba, M.G. Betigeri, M. Bharati*, B. Lal* and N.G. Puttaswamy** - A systematic investigation of properties of low lying levels of nuclei in the region $28 \leq Z \leq 40$ and $40 \leq N \leq 50$ is being undertaken. As a part of the prog: .mme, we have studied the conversion electrons and gamma rays following (p,n) reactions on ^{80}Se, $^{79,81}Br$ targets. Typical γ -spectrum and conversion electron spectra for $^{79,81}Br(p,n)^{79,81}Kr$ reactions are shown in Fig.5 . By suitable normalization for the 130 keV - transition in ^{79}Kr, which is measured to be E3, we have obtained absolute K-conversion coefficients which are listed in Table 3. The results for $^{80}Se(p,n)^{80}Br$ are being analysed.

6. <u>Study of ^{75}Se through $^{75}As(p,ne)$ Reaction</u> - Y.K. Agarwal*, C.V.K. Baba, S.M. Bharati*, S.K. Bhattacharjee*, B. Lal* and Baldev Sahai* - In view of the large observed quadrupole moment for the ground-state of ^{75}Se and also the fact that its ground state spin of $5/2^+$ differs from the value predicted by the single particle shell model, it is interesting to study its level scheme. Recently Baldev Sahai and B. Lal[1] have made a detailed study of the level structure of this nucleus through $^{75}As(p, n\gamma)$ reaction and also measured the angular distribution[2] of γ -rays. The present study was undertaken to supplement this data with the information about the multipolarities and lifetimes of some of the lowlying levels in ^{75}Se.

---

* Members of Tata Institute of Fundamental Research.
** Department of Physics, Bangalore University.

The internal conversion electrons arising from the $^{75}As(p,n)$ reaction were detected by a six-gap β-ray spectrometer[3)] installed at Van de Graaff, Trombay. Arsenic targets of $\sim$ 200 μgm/cm^2 thickness on thin carbon backing were used for this purpose. The conversion electron spectra of 112, 133, 141, 287, 377, 428 and 516 keV transitions have been recorded at proton energies of 2.7, 3.5 and 5.0 MeV. A 5 c.c. Ge-Li detector on top of the spectrometer facilitated the simultaneous recording of γ-ray spectra. A typical conversion electron spectrum taken at Ep = 5.0 MeV is shown in fig. 6 . Table 4 gives the K-conversion coefficients for the above transitions obtained from the present measurements. The assigned multipolarities are based on comparison of the measured conversion coefficients with the theoretical values.

Lifetimes of 112, 133 and 287 keV levels were obtained by making delayed coincidence measurements between the K-conversion electrons feeding or emanating from the levels and the corresponding cascade γ-rays. 1" x 1/2" plastic and 1 3/4" ø x 1" NaI crystal served as the electron and γ-ray detectors respectively. Fig.7 shows the lifetime curve for 287 keV level.

A gamma ray of 133 keV could be seen from Ep = 2.5 MeV onwards in thin target spectra. However, at lower proton energies, this was masked by the 136 keV γ-ray line arising from β-decay of ^{75}Se activity and also from $^{75}As(p,p')$ reaction. The K-conversion electron line corresponding to 133 keV gamma ray could be very clearly seen with the spectrometer. The excitation function for this transition has also been measured to find out its threshold. The threshold comes out to be 2.2 MeV.

The level scheme of ^{75}Se is given in ref.2. From the earlier measurements[1], the angular distribution of γ -rays[2] and the present data on conversion coefficients, the following spin and parity assignments could be made: 112(7/2$^+$), 133(9/2$^+$), 287(3/2$^-$), 428(5/2$^-$) and 664(5/2$^-$). An upper limit for the lifetime of the 112.0 keV is found to be about 0.8 nsec which is consistent with the predominantly M1 character of the transition. The 287 keV level has $T_{1/2}$ = 1.2 $\pm$ 0.1 nsec. This differs from single particle estimates by a factor of $\sim 10^5$. The 133 keV level has $T_{1/2}$ = 4.13 $\pm$ 0.7 ns.

1) Baldev Sahai, B. Lal, Proc. of Nucl. Phys. Symposium, India, Vol.2 (1970)

2) B. Lal and Baldev Sahai, to be published in Proc. of Nucl. Phys. Symposium, India, Vol.2 (1972)

3) S.K. Ambardekar, C.V.K. Baba and S.M. Bharati, Proc. of Nucl. Phys. Symposium, India, (1969).

Table 4

Transition Energy (keV)	α_K	Multipolarity
112	$(1.04 \pm 0.07) \times 10^{-1}$	M1 + 9% E2
133	$(1.37 \pm 0.10) \times 10^{-2}$	E2
141	$(2.40 \pm 0.19) \times 10^{-2}$	M1
287	$(3.01 \pm 0.19) \times 10^{-3}$	E1
377	$(4.72 \pm 0.97) \times 10^{-3}$	M1 + 54% E2
428	$(9.57 \pm 3.35) \times 10^{-4}$	E1
516	$(1.88 \pm 0.16) \times 10^{-3}$	M1 + 58% E2

7. <u>Excitation Function for the Gamma-ray Yields From Alpha Particle Bombardment of 19 F in the Range 3.96 to 4.55 MeV</u> - M. Balakrishnan, M.K. Mehta and A.S. Divetia - Low-lying levels in ^{23}Na have been studied extensively[1]. In recent years Dubois[2] has investigated the levels in ^{23}Na upto an excitation of 7.75 MeV in a study of the reaction ^{25}Mg(d,α)^{23}Na. He extracted a nuclear temperature of 2.1 MeV from his data and found that the level density for ^{23}Na agreed with that of ^{23}Mg in the same region of excitation. There has been little information on the energy levels above 7.75 MeV excitation except that from the work of Freeman and Mani[3]. They have made a study of the yield of gamma rays following the bombardment of alpha particles on ^{19}F targets for incident energies ranging from 3.95 to 4.55 MeV. They used a NaI(Tl) crystal to detect the gamma rays. We have undertaken a study in this region of excitation through the incident channel ^{19}F + α , with a view to get more detailed information by employing higher resolution ($\sim$7 keV) as well as measuring more exit channels utilizing a Li drifted Ge detector.

About 0.1μA analyzed beam of He$^+$ ions was used to bombard a ^{6}LiF target. A 30 cms diameter scattering chamber[4] with an aluminium window about 340 microns thick for mounting a Ge(Li) detector was used for this purpose. The gamma rays were detected by a 30 c.c. Ge(Li) detector kept at 80° forward angle at a distance of 2 cms from the target. Charged particles resulting from the bombardment were also detected by solid state detectors at three backward angles. However, the charged particle results are not reported in this paper. The signals from the Ge(Li) were fed into a 4096 channel analyser using conventional electronics. Following are the energies of the gamma rays identified in the resulting spectrum; 110 and 197 keV resulting from the inelastic scattering, 1.275 and 2.073 MeV from the (α, p_1) and (α, p_2) reaction and 583 and 891 keV from the (α, n_1) and (α, n_3) reactions. Excitation functions were measured for these gamma rays over the bombarding energy range 3.96 to 4.55 MeV. A large number of resonances, 36 in all, are observed indicating a high level density in the compound nucleus ^{23}Na. The excitation functions are shown in fig. 9 . The presence or absence of some of the resonances in different channels indicate highly selective decays of the corresponding levels in ^{23}Na.

Any meaningful analysis of this data in terms of level widths and level separation requires a knowledge of the energy loss of the alpha particle beam in the target material. This was determined by measuring the experimental width of a resonance in the $^{6}Li(\alpha, \alpha)^{6}Li$ reaction at a bombarding energy of 2.80 MeV from previous work[5]. The measurement is shown in Fig. 8 . From this an energy loss of 7 ± 1 keV for 4 MeV alpha particles was measured to be the effect of the target thickness.

The experimental widths (Γ) and the level positions (E_R) were extracted by fitting a Lorentzian under each observed peak (including weak ones) so that the cross section between two peaks was given by the sum of the two or more Lorentzians underneath. This procedure is justified within the accuracy of the estimates made here (± 25%) as the very large solid angle subtended by the detector will virtually integrate over any kinematic interference effects. The dynamic interference due to two levels of the same spin and parity occuring within a spacing of about 7-10 keV is likely to modify the Lorentzian shape only marginally. The observed level spacing (S) distribution with bin size of 4 keV is shown in Fig. 10 . The maximum occuring at a finite spacing S around 12 keV is evident. The curves show the expected Wigner $\left\{\frac{\pi}{2}\frac{S}{\bar{S}^2}\exp\left(-\frac{\pi}{4}\frac{S^2}{\bar{S}^2}\right)\right\}$ or a similar realistic distribution, as well as the exponential distribution which clearly is not the right one for the observed spacings. The observed level density of 61 levels/MeV was converted to nuclear temperature by means of the expressions $W(E) = Ce \times p2(aE)^{1/2}$ and $E = a\theta^2$ with $C = .55\ \mathrm{MeV}^{-1}$. A value of 5.5 MeV for the temperature θ obtained this way agrees with known values for similar mass number in the region of excitation of 14 MeV.

As a large number of channels are open in this region of excitation, the total decay width of each level may be made up of a large number of partial widths roughly equal in magnitude. If such is the case the yield in each channel for a particular resonance will largely be governed by the penetrabilities involved in the exit channel. These penetrability calculations are complete and indicate differences of an order of magnitude between different values of ℓ . It is hoped that by comparing these with ratios of the yield, some rough assignments for the spin and parity of the levels would be made or limits would be established.

1) P.M. Endtland C. Van Der Leun, Nucl. Phys. A105(1967)26

2) J. Dubois, Nucl. Phys. A99(1967)465

3) R.M. Freeman and G.S. Mani, Nucl. Phys. 51(1964)593

4) M. Balakrishnan, described else where in this report.

8. <u>Transient fields on ^{56}Fe in Fe at Low Recoil Energies and g Factors of First 2^+ States in ^{108}Pd, ^{110}Pd and ^{104}Ru</u> - Y.K. Agarwal[@], A.P. Agnihotry*, C.V.K. Baba, S.K. Bhattacherjee*, H.C. Jain*, M.C. Joshi* and P.N. Tandon* - g-factors of many vibrational states have been measured recently using IMPAC techniques[1)]. In almost all these experiments the recoil energies are quite large (~ 16 MeV) and transient field effects are quite predominant in many cases involving states having extremely short half-lives[1)]. A series of experiments, in which the recoil energies were much lower, were carried out with a view of determining g-factors with lesser ambiguities.

g-factors of first 2^+ states in ^{108}Pd, ^{110}Pd, ^{104}Ru were measured using techniques similar to those described earlier[2)]. Iron alloys with 20 at.% Pd and 5 at.%Ru were used in the present experiment. A 5 MeV α -beam was used to Coulomb excite the levels. Two Ge(Li) detectors, one 20 c.c. and the other 30 c.c. were used for measuring R. These detectors were located at 135° and 225° with respect to the beam. The field at Pd in the alloy used was measured in a separate experiment by utilising the known g-factor of the 512 keV state in ^{106}Pd. Mossbauer effect was used to determine the field at Fe in the Pd Fe alloy. Table 5 shows the results of the R measurements. The value of A_2 were measurd using one detector only by varying the angle from 90° to 270° in 15° steps.

<u>Table 5</u>

State	T 1/2	R	$\omega\tau$	g
847 keV ^{56}Fe	7.8 ps	0.36 ± 0.14 %	4.4 m Rad	0.51**
374 keV ^{110}Pd	45 ps	1.77 ± 0.13 %	27.2 m Rad	0.23 ± 0.05
434 keV ^{108}Pd	25 ps	1.04 ± 0.14 %	16.0 m Rad	0.27 ± 0.08
360 keV ^{104}Ru	54 ps	3.02 ± 0.25 %	46.5 m Rad	0.28 ± 0.04

* Members of Tata Institute of Fundamental Research

**Value measured by Appel and Mayer from radioactivity work and used here for determining transient field effect.

In the case of ^{56}Fe the g-factor has been measured from radio-activity work[3] and thus the contribution due to transient field to $\omega\tau$ is found to be

$$\omega\tau'_{trans} = 4.8 \pm 3.4 \text{ m Rad.}$$

The measured values of $\omega\tau$ for the Pd and Ru states have to be corrected for transient field effects. According to Lindhard & Winther[4] transient field is proportional to Z. Using the theory of slowing down and the values of recoil energy for Fe, Pd and Ru the transient field effects for Pd and Ru are computed to be

$$\omega\tau_{trans} = 6 \pm 3 \text{ m Rad for Pd}$$

$$= 6 \pm 3 \text{ m Rad for Ru.}$$

The g-factors derived from the corrected $\omega\tau$ values are also given in Table 5. These results are in very good agreement with earlier work.[5]

1) L. Grodzins in Hyperfine Structure & Nuclear Radiation - North Holland, Amsterdam (1968)607.

2) S.K. Bhattacherjee, H.G. Devare, H.C. Jain, M.C. Joshi and C.V.K. Baba, Hyperfine Interactions in Excited Nuclei - Gordon&Breach, London (1971)1081
H.C. Jain, Ph.D. Thesis (1971), Bombay University, unpublished

3) H. Appel and W. Mayer, Nuclear Physics 43(1963)393

4) J. Lindhard and A. Winther, Nuclear Physics A166(1971)413

5) G.M. Heestand, R.R. Borchers, B. Herskind, L. Grodzin, R. Kalish and D.E. Murmick, Nuclear Physics A133(1969)310

9. Spins of Low Lying Levels in ^{75}Se - B. Lal* and Baldev Sahai° -

In continuation of our earlier work on the level scheme of ^{75}Se, angular distribution of 112, 141 and 428 keV transitions at an average bombarding energy Ep = 2.37 MeV and those of 377, 611 and 628 keV transitions at an average bombarding energy Ep = 2.635 MeV have been carried out using 30 c.c. Ge(Li) detector for gamma ray detection. By comparing

*Members of Tata Institute of Fundamental Research experimental angular distribution with the calculations based on Sheldon's formalism (Rev. of Mod. Physics 38(1966)145), of Hauser-Feshbach statistical model, the χ^2 vs $\tan^{-1}\delta$ for each of the transitions have been plotted (see fig. 11). The results for the spins of various levels derived on the basis of 0.1% confidence limit for the χ^2 fit are summarized in Table 6.

Table 6

Initial State (keV)	Assigned spin	Final stage E(keV)	J	Mixing ratio
112	7/2	g.s	$5/2^+$	$-0.09^{+0.03}_{-0.04}$ or $-3.27^{+0.46}_{-0.37}$
428	(7/2, 5/2, 3/2)	287	$3/2^-$	Unconstrained
428	(7/2, 5/2, 3/2)	g.s	$5/2^+$	Unconstrained
611	7/2	g.s	$5/2^+$	-0.035 to +0.18
	(5/2)			-0.36 or +5.7
	(9/2)			-2.14 to -2.75
628	7/2	g.s	$5/2^+$	-11.4 to +0.14
	(5/2)			-0.47
	(9/2)			-0.36 to - 2.75
664	5/2	287	$3/2^-$	-0.02 to + 2.75

10. The 6.88 MeV Level in ^{10}B - M. Balakrishnan, S. Kailas, L. Kanetkar*, C.V. Fernandez and M.K. Mehta - The 6.88 MeV level is known to be of $J^{\pi} = 1^-$ and is having the highest isospin impurities of the known levels in light nuclei. To confirm the properties of this level through the elastic scattering of alpha particles, preliminary scattering experiments were made on enriched ^6Li targets in ^6LiF form on very thin carbon backings. The angles of scattering were 135°, 114°, 84° and 56° in the lab system. The target thickness used was about 7 keV for 3.5 MeV alphas. Since this level is known to have relatively smaller alpha width the elastically scattered yield was

*University of Bombay student

relatively low but very good spectra were obtained, since the target used was thin. There is some indication for existance of anomalies in the excitation function in the region 3.9 to 4.3 MeV incident alpha energies, which are not yet reported in the literature and hence further studies are planned in this region.

11. <u>Calculation of doorway States in Elastic Scattering</u> - S.S. Saini and S.K. Gupta - Using Payne's[1)] formalism for the calculation of isolated bound door way states occuring in neutron elastic scattering, a computer program has been written to calculate the doorway state energies for single closed shell (S.C.S.) nuclei. The door way state energy Ed is given by

$$E_d = E_o + \langle 3QP \mid H^{22} \mid 3QP \rangle - B_n \qquad (1)$$

where E_o is the sum of the three quasiparticle energies, B_n is the neutron-separation energy of the (A + 1) compound nucleus. In writing the expression (1) we assume that all the energies are measured from the top of the potential well.

The matrix element $\langle 3QP \mid H^{22} \mid 3QP \rangle$ is calculated using harmonic oscillator wave functions. A closed expression was found for calculating the radial integrals as is given below

$$I(R_{n_1l_1}R_{n_2l_2}R_{n_3l_3}R_{n_4l_4}) = \frac{(2\nu)^{3/2}}{\sqrt{2\pi}} 2^{\frac{1}{2}(2 - \sum_{i=1}^{4} l_i - \sum_{i=1}^{4} n_i)} \times$$

$$\left\{ \prod_i \left[\frac{(2l_i + 2n_i + 1)!!}{\sqrt{n_i}} \right]^{1/2} \times \sum_{k_1}^{n_1} \sum_{k_2}^{n_2} \sum_{k_3}^{n_3} \sum_{k_4}^{n_4} (-)^{k_1+k_2+k_3+k_4} \, 2^{-\sum_{i=1} k_i} \times \right.$$

$$\left. \left[\left\{ \sum_{i=1}^{4} (l_i + 2k_i) + 1 \right\} !! \right] \times \prod_i \left[\binom{n_i}{k_i} \frac{1}{(2l_i + 2k_i + 1)!!} \right] \right\} \qquad (2)$$

The quasi particle energies were calculated using a code QUASI which solves two coupled equations in chemical potential λ and half gap energy Δ starting from approximate values of λ and Δ and the single particle energies. The quasi particle energy is given by

$$E_j = \sqrt{(\epsilon_j - \lambda)^2 + \Delta^2} \tag{3}$$

where ϵ_j are single particle levels. λ and Δ are found by solving the following equations for λ and Δ simultaneously.

$$\frac{|G|}{2} \sum_j \frac{\Omega_j}{\sqrt{(\epsilon_j - \lambda)^2 + \Delta^2}} = 1 \tag{4}$$

$$\sum_j \Omega_j \left[1 - \frac{\epsilon_j - \lambda}{\sqrt{(\epsilon_j - \lambda)^2 + \Delta^2}} \right] = N \tag{5}$$

where G is the pairing interaction, Ω_j is the pair degeneracy of the single particle levels and N is the average number of nucleons outside the closed core.

Slight manipulation of these equations gives the exact values of λ and Δ as

$$\lambda = \frac{|G|}{2} \left[n - \sum_j \Omega_j + \sum_j \frac{\Omega_j \epsilon_j}{E_j} \right] \tag{6}$$

$$\Delta = \frac{|G|}{2} \sum_j \Omega_j \left\{ 1 - \frac{(\epsilon_j - \lambda)^2}{E_j} \right\}^{1/2} \tag{7}$$

To start this iteration process we start from approx values of λ and Δ

$$\lambda = \frac{|G|}{2} N$$

$$\Delta = \frac{|G|^2}{4} N (2\Omega - N), \quad \Omega = \sum_j \Omega_j$$

These calculations will be extended to proton scattering.

1) G.L. Payne, Phys. Rev. 174(1968)1227

12. Absorption of 2P Pions Followed by the Emission of Two Neutrons - B.K. Jain - Since the measured recoil momentum distribution in (π^-, nn) reaction does not discriminate amongst the contribution from the different pionic orbits, experimentally observed transition strength is equal to the weighted average absorption strength from various orbits. If we assume that the absorption from orbits other than 1S and 2P are negligible,

$$Y_{exp}(2n) = \frac{W_{2p}(2n)}{W_{2p}^a + W_X} + \frac{W_X}{W_{2p}^a + W_X} \quad \frac{W_{1S}(2n)}{W_{1S}^a}$$

where Y_{exp} is the experimental yield of nn, W_{nl}^a is the total absorption rate for the nl orbit and W_X is the X-ray transition rate from 2P to 1S orbit. W^a can be deduced from the intensity attenuation of X-rays. If we substitute values for various terms for ^{12}C,

$$Y_{exp}(2n) \propto (W_{2p} + 0.4 \times 10^{-4} \; W_{1S})$$

However, due to the strong overlap of the pion wave function with the nuclear wave function, W_{1S} is about 10^4 times larger than W_{2P} This is compensated by the 10^{-4} factor appearing with W_{1S}. Therefore, the contribution of 2P and 1S pion in ^{12}C nucleus is comparable. We have done the calculations for ^{12}C nucleus including the contribution of both the 1S and 2P pions. The computed results are compared with the experimental data of Cheshire and Sobottka. It is found that the agreement is good for the absorption of pions on $(1s)^2$ nucleons. For the absorption on $(1p)^2$ nucleons the agreement becomes bad. For these nucleons the computed results agree very well with the experimental data if the absorption of only 1S pions is considered.

13. <u>Pion Absorption and the Structure of ^6Li Nucleus</u> - B.K. Jain - The available data on $^6Li(\pi^-,nn)$ reaction are analysed using the formalism we had developed earlier. The pions in 1s orbit are described by the Seki-Cromer wave function. For the ^6Li the cluster model wave functions are used. The parameters of this wave function are taken from the literature where they fit the binding energy, quadrupole moment, charge form factor and the (p,pd) reaction data on ^6Li. It is found that for (π^-,nn) reaction these wave functions give a recoil momentum

distribution which falls off rather too rapidly. Furthermore, while studying the sensitivity of the recoil momentum distribution to the inter cluster wave function, it is observed that it depends on the inter cluster wave function only beyond 4.0 fm. It is suggested that the discrepancy between the calculated and observed distribution may be removed if the mechanism of both the reactions (π^-,nn) and (p,pd) are made little more sophisticated.

To be published in the Proceedings of Nuclear Physics and Solid State Physics Symposium, (India) 1972.

14. <u>DWIA Program for the (p,2p) Reaction in the Energy Region of 200 - 1000 MeV</u> - B.K. Jain and R. Shanta* - A report, which describes the DWIA (Distorted Wave Impulse Approximation) computer program for CDC-3600 in FORTRAN for the analysis of the (p,2p) reaction in the co-planar symmetric geometry, is prepared. The program uses the di-proton model for the description of the final state, WKB approximation for the incoming and outgoing distorted waves, and relativistic kinematics. As these approximations are valid only at high energy, this code is suitable for calculations in the 200 - 1000 MeV region of incident proton energy.

The program evaluates the differential cross-section except for the spectroscopic factor S_{fi}. The S_{fi} can be obtained by fitting the experimental data. The bound state wave function is considered as input. Hence it is useful to study the effect of different bound state wave functions.

---

*Visiting member during 1969-70
To appear as BARC Report, 1972.

15. <u>Investigation of Alpha-Triton Clustering in ^{7}Li by $^{7}Li(p,pt)^{4}He$ Reaction</u> - A.K. Jain and N. Sarma - A relatively small t-α separation energy makes the ^{7}Li nucleus interesting from the point of view of cluster model. The study of such clustering phenomenon should be possible through cluster knock-out reactions. Therefore the reaction $^{7}Li(p,pt)^{4}He$ has been analysed using completely antisymmetrized cluster model wave functions in the distorted wave impulse approximation (DWIA). The intercluster wave function used in this work has an exponential asymptotic behaviour corresponding to the α-t separation energy. The distortions of the scattering states have been found to fill up the valley in the angular correlations and suppress the lower angle peak by sizable amount. Though the effect of exchange terms has been of opposite nature on 156 MeV and 55 MeV calculations it is of less importance in deciding the shape of the angular correlation curves because of smaller magnitude of such terms. The calculations reproduce both the magnitude and shape of the angular correlation data at 156 MeV. It is very encouraging to note that without the introduction of any free parameters the same formulation fits the data at 55 MeV as well.

16. <u>Parameterisation of the Elastic Scattering of ^{28}Si from ^{28}Si with Nuclear Optical Model</u> - S.S. Saini and M.K. Mehta - Calculations are taken in hand to fit the data obtained at Chalk River Nuclear Laboratory by Hausser et al.[1] on the reaction $^{28}Si(^{28}Si,^{28}Si)^{28}Si$ using the programme LMOP obtained from the University of Washington[2]. This programme is specially written to deal with the scattering of identical particles and has a provision to include an ℓ dependence for the imaginary part of the optical potential as suggested by the

F.S.U. Group[3]. Hausser et al. fitted their angular distributions obtained at the c.m. bombarding energy of 20, 25, 30, 35 and 40 MeV by the simple Blair Model[4]. Our preliminary results suggest that the relatively shallow (30 MeV) optical potential used around this region of mass for the heavy ions do not produce good fits to the data, if ℓ dependence is not included. A set with very deep real potential ($\sim$180 MeV) does produce a good fit at lower energies, however, this value is considered unrealistic. The effect of including the ℓ dependence of the imaginary potential is now being investigated.

1) O. Hausser, T.K. Alexander, A.J. Ferguson and A.B. Mac donald, Bull. Am. Phys. Soc. II, 15(1970)630

2) This programme has been written by R.W. Shaw (Jr.) of University of Washington, Seattle, U.S.A.

3) R.A. Chatwin, J.S. Eck , D. Robson and A. Richtor, Phys. Rev. C1(1970)795

4) J.S. Blair, Phys. Rev. 108(1967)827

17. Hartree-Fock-Bogoliubov Calculations for Even-Even Nuclei in p-f Shell - Jyoti K. Parikh - Hartree-Fock-Bogoliubov (HFB) calculations are done for some even-even nuclei in the p-f shell taking ^{10}Ca as a doubly closed core. It is observed that the nuclear shape changes from a prolate to oblate shape, and the pairing correlations increase in the neutron states and decrease in the proton states as one goes from the Ti to the Zn and Ge isotopes. Whether the $f_{7/2}$ shell-closure approximation in which ^{56}Ni is taken as a closed core is valid or not is discussed by comparing the calculated occupation probabilities of the $f_{7/2}$ shell and the break in the pair separation energy at ^{56}Ni with the experimental values. Projected HFB spectra have been obtained for ^{64}Zn, ^{66}Zn and ^{70}Ge. Reasonable agreement with the experimental spectra

is obtained for ^{66}Zn and ^{70}Ge. The reasons for the failure of the persent method in ^{64}Zn are discussed.

18. Hartree-Fock-Bogoliubov Calculations for the odd Nuclei - Jyoti K. Parikh - Hartree-Fock-Bogoliubov (HFB) method is a powerful method if one wants to handle many nucleons outside the closed core in a reasonable configuration space, to consider deformation and to include the pairing correlations.

Encouraged by the success in the even-even nuclei HFB equations are reformulated to be able to extend them to add nuclei as well. The blocking effect due to the odd nucleon is taken into account in the wave function given by

$$\psi = \frac{b_i^+ + b_{\bar{i}}^+}{\sqrt{2}} \prod_{j \neq i, \bar{i}} (u_j + V_j b_j^+ \; b_{\bar{j}}^+) \, |0>$$

Here i (or $\bar{i}$) is used to denote the state which is occupied by the odd nucleon, j refers to all the states other than i state. b^+ are the creation operators in the deformed basis. In order to solve for ψ, we make the usual quasi particle transformation. On making this transformation, it could be shown that the density matrix is hermitian in the spherical basis.

Similarly, the pairing tensor t is antisymmetric and can be reduced to a block form in the deformed basis. Taking the expectation value of H and using Wick's theorem, and minimizing using iterative procedures one obtains the selfconsistent solutions. One finds that i and j states influence each other by HF potential only, whereas j states interact among themselves through HF as well as the pairing potential. Minimizing H with respect to U_j, V_j the deformation coefficients C^K, one obtains the equations for C^K and the quasiparticle energies.

The numerical calculations are carried out using the parameters given in ref. 1), but the single particle energies taken now are somewhat modified for the neutrons and for the protons 7 MeV is added to account for the Coulomb repulsion. The results for the binding energies, separation energies and the pair separation energies are given in Table 7. The intrinsic quadrupole moments are also given. The calculations for the moments of the ground state and first excited states and BE2 are in progress.

Table 7

The binding energies, the neutron separation energies and the pair separation energies are given in MeV. The relative intrinsic quadrupole moments are given.

Nucleus	Binding energy		sep. energy		pair sep. energy		Intrinsic
	Calc.	exp.	calc.	exp.	calc.	exp.	Q
^{46}Ti	394.6	398.2	-	-	-	-	19.5
^{47}Ti	405.0	407.1	10.4	8.9	-	-	21.1
^{48}Ti	415.4	418.7	10.4	11.6	20.8	20.5	17.6
^{49}Ti	425.1	426.9	9.7	8.2			16.2
^{50}Ti	435.7	437.8	10.6	10.9	20.3	19.1	11.9
^{51}Ti	443.8	444.2	9.4	6.4			13.6
^{50}Cr	432.0	435.0	-		-		24.6
^{51}Cr	441.4	444.3	11.2	9.3			16.8
^{52}Cr	453.3	456.3	12.4	11.2	21.1	21.3	21.9
^{53}Cr	462.8	464.3	9.5	7.9			28.3
^{54}Cr	473.9	474	11.1	9.7	20.6	17.7	23.7
^{55}Cr	482.3	480.2	8.4	6.3			21.4
^{54}Fe	470.4	471.7	-		-		2.8
^{55}Fe	480.5	481	10	9.3			14.8
^{56}Fe	492.2	492.2	11.2	11.2	21.8	20.5	10.4
^{57}Fe	501.9	499.7	9.7	7.6			24.8

1) Jyoti K. Parikh, Phys. Rev. 5C(1972)153

19. <u>The Electromagnetic Properties and the Spectroscopic Factors of the p-f Shell Nuclei</u> - Jyoti K. Parikh - The calculations of the electromagnetic properties of nuclei provide a sensitive test for a given nuclear model. The sign and magnitude of the quadrupole moment of the first excited state (Q_2+) in the case of an even-even nucleus gives information about the nuclear shape and the amount of deformation respectively. BE_2 values are proportional to the square of the matrix elements and hence are more sensitive to the wave function than the nuclear spectra. For this reason, BE_2 and Q_{2+} are calculated employing the HFB wavefunctions with which good agreements with spectra and binding energies are obtained earlier. The comparison of the values given by the simple shell model, projected Hartree-Fock (PHF) method, the present method (PHFB) and the experimental data is given in Table 8.

The spectroscopic factors contain vital information obtained from the one nucleon transfer reactions. They indicate the amount of configuration mixing which should be simulated by a given two-body force and shed light on the validity of the closure approximations, e.g. the present study shows that to take ^{56}Ni is not a valid approximation by showing that there exist holes in the $f_{7/2}$ shells for these isotopes.

The occupation probabilities obtained from the present calculations are given in Table 9.

Table 8

	$(BE2)_{exp.}/(BE2)_{s.p}$	PHF ($e = .31$)	PHFB ($e = .2$)	Exp.
^{46}Ti	14	4.2	6.6	8 ± 1.7
^{48}Ti	13	3.6	5.06	7 ± 1.4
^{50}Ti	6	2.4	2.0	3.2 ± .8
^{50}Cr	25	7.4	11.1	12 ± .8
^{52}Cr	-	5.6	5.3	6.7 ± .7
^{54}Cr	-	7.4	8.6	10 ± .7
^{54}Fe	-	5.2	4	5.1 ± .5
^{56}Fe	-	6.8	8.7	9.0 ± 1

2nd column indicates the ratio of $(BE2)_{exp.}$ and BE2 obtained from the single particle shell model. The 3rd column indicates the PHF results modified by taking the correct radius 3.6 fm^2. The present results PHFB are obtained by taking $e = .8$ where e is the effective charge.

Table 9

Occupation Probabilities

	Protons				Neutrons			
Nucleus	$p_{1/2}$	$p_{3/2}$	$f_{5/2}$	$f_{7/2}$	$p_{1/2}$	$p_{3/2}$	$f_{5/2}$	$f_{7/2}$
Ti^{46}	.11	.42	.15	1.32	.13	.50	.22	3.10
Ti^{48}	.08	.32	.13	1.46	.12	.51	.25	5.07
Ti^{50}	.05	.21	.11	1.62	.10	.49	.24	7.12
Cr^{50}	.13	.81	.16	2.92	.45	1.0	.72	3.88
Cr^{52}	.10	.76	.11	3.04	.52	1.04	.86	5.55
Cr^{54}	.08	.57	.10	3.27	.46	1.0	.91	7.63
Fe^{54}	.68	1.31	.79	3.22	.66	1.28	.95	5.18
Fe^{56}	.30	.89	.48	4.33	.53	1.1	.84	7.52
Fe^{58}	.27	1.01	.21	4.51	.72	2.12	1.59	7.57
Ni^{58}	.50	1.18	.72	5.6	.57	1.18	.80	7.45
Ni^{60}	.68	1.64	.19	5.50	.83	2.18	1.95	7.1
Ni^{62}	.38	1.96	.17	5.48	.93	2.55	2.75	7.76
Ni^{64}	.18	1.97	.08	5.77	1.44	3.64	3.04	7.87
Zn^{64}	.93	2.4	.61	6.1	1.30	2.66	2.7	7.3
Zn^{66}	.71	2.6	.28	6.4	1.5	3.61	3.0	7.8
Zn^{68}	.32	2.47	.11	7.1	1.56	3.72	4.8	7.9
Ge^{70}	.57	3.6	.1	7.7	1.96	3.98	4.11	7.94

INSTRUMENTATION

1. A Fast Neutron Time-of-flight Spectrometer for Use in Neutron Gamma Ray Coincidence Experiments - N.L. Ragoowansi and M.A. Eswaran - For use in neutron gamma ray coincidence experiments in nuclear reactions a fast neutron time-of-flight spectrometer arrangement has been set up. A plastic scintillator mounted on XP1040 phototube is used for neutron detection and NaI(Tl) scintillation counter is used for gamma rays. The main part of the system is a transistorised time-to-amplitude convertor which is built based on the circuitry published in reference[1]. This incorporates in addition to the time-to-amplitude convertor, a fast coincidence arrangement which triggers the T.A.C. enabling the timesorter to be operated by only the coincident events. The block diagram of the apparatus is shown in Fig.12 . Using neutron gamma ray coincidence from the reaction $^{9}Be(\alpha,n\gamma)^{12}C$ from Am-α-Be source the performance of the above system has been checked employing various flight paths. The examples of the such time-of-flight spectra are shown in Fig. 13 . This system is also useful in general coincidence experiments for recording random and true plus random spectra simultaneously.

1) R.B. Tomlinson and R.L. Brown, IEEE Trans. on Nucl. Sci., April 1964, p.28.

2. Stabiliser for PN400 Accelerator - M.S. Bhatia - A prototype of terminal voltage stabiliser has been designed and built. It is a three stage differential amplifier which compares a voltage developed across a resistance in series with the column current of the accelerator with the voltage from a standard cell of 1.5V. The output of

this amplifier controls the corona series tube and thus controls the terminal voltage.

The system has been incorporated in PN 400 Van de Graaff accelerator. Its stability has been found to be better than ± 0.5KV. At present different values of column current series resistor are to be used for accelerator terminal voltage changes of more than 100 KV. Work is in hand to build a more precise stabiliser which will give a stability within ± 100 volts and do away with the need of changing this resistor.

3. Non Linear Effects in the Van de Graaff Analysing Magnet - S.S. Kerekatte, M.S. Bhatia and M.K. Mehta - A discrepancy was noticed in the values of energies at which resonances were observed in the study of the reaction $^{24}Mg(\alpha, \alpha)^{24}Mg$ at this laboratory as compared to the same resonances observed at some other laboratory. A study was undertaken to trace the source of this discrepancy. It was observed that the magnitude of the discrepancy was proportional to the nominal energy itself, i.e. resonances in the same reaction but at energies around 3.5 MeV agreed within 10 keV with previous values while around 5.5 MeV the disagreement was as much as 120 keV. This could be only due to the saturation effects setting in, which made the magnetization curve nonlinear at fields considerably lower than where it was expected. The magnet was then tested for nonlinearity and local effects by placing the NMR probe at a number points within the gap and by observing the local field variation as a function of magnet current. The results indicated that the local field against current variation started deviating from linearity at a field which corresponds to about 4.00 MeV alpha particle beam energy. The magnet saturates around 13.5 kilo-

gauss. Experiments are underway to systematically investigate this effect utilising resonances and thresholds for a number of nuclear reactions. Once complete, this will yield corrections required for energy values when singly charged ^{4}He and ^{3}He beams are used.

4. <u>Performance Testing of the New Ion Source Beam Filter Assembly Installed in the Van de Graaff Terminal</u> - S.N. Misra, S.S. Kerekatte, M.K. Mehta, S. Kailas, S.K. Gupta, L. Kanetkar* and M.S. Bhatia - The pre-injection e/m analyser system described in an earlier report[1)] has been installed in the terminal of the Van de Graaff accelerator. The preliminary performance tests have yielded an $^{4}He^{+}$ current of more than 5 μ amp of analyzed beam at a typical energy of 3.5 MeV on the beam stopper. With the same setting of the terminal voltage an analysed beam current of 70 μ amp has been measured onthe beam stopper with the 90° analysing magnet set for 7 MeV $^{4}He^{++}$ energy. Experiments are in progress to identify this beam as the alpha particle beam through known nuclear reactions. As there is a probability for an HH^{+} beam of 3.5 MeV energy to pass through the analysing magnet at the same setting, a test through nuclear reactions is necessary before a positive identification can be made. The performance of the beam filter-ion source assembly after installation at site has not changed much from its performance on the bench set up. It is expected that high beam currents for all particles (except the He^{++}) will be available and the installation of this system can be considered as a first step towards installation of a nanosecond pulsed beam facility.

1) Annual Report of the Nuclear Physics Division - 1970, B.A.R.C-557(1971)23

* University of Bombay student

5. <u>A Preset Scaler Control Unit for Data Recording System</u> - V. Tamwekar and S.S. Kerekatte - A transistorized preset scaler has been built and tested for automation in nuclear data collection. The automation is achieved by controlling a pulse height analyser and an electric timer for a preset range of counts which extend upto 10^8 counts. This instrument is useful in the precision measurement of nuclear reaction cross-sections.

6. <u>Beam Profile Scanner</u> - C.V. Fernandes and S.S. Kerekatte - A beam profile scanner has been designed and partly assembled. This instrument will display the beam profile along two axes at right angles to each other. The profile will be displayed on a dual trace oscilloscope in the control room and help in remote control of the beam steering parameters such as deflection and focus.

7. <u>Scattering Chambers</u> - M. Balakrishnan and C.V. Fernandes - i) A 12" scattering chamber was built which accommodates charge particle detectors along with a Ge-Li gamma ray detector. There is a well type window 6.35 cm in diameter at 80° forward angle, made of 0.38 to 0.43 mm thick aluminium, so as to reduce the absorption of the gamma rays at the window. The depth of the window is such that a 30 c.c. Ge(Li) detector placed in it will be very near the target (about 1.5 cms). There is provision for only one target mounting support. However, two target frames can be mounted one above the other on this support. A good liquid nitrogen trap which need refilling once in 24 hours, is mounted on top of the scattering chamber, so that the cooler bottom region of the trap extends very close to the target position. This helps in reducing the carbon build up on target considerably. The chamber has already been put to use.

ii) A versatile 24" scattering chamber, which takes into account many of the draw backs of the scattering chambers which are in general use in the laboratory, has been designed and the fabrication is in progress. The central cylindrical portion of the chamber has already been completed.

The following are the major features of this chamber:

a) All the accurate geometries of the chamber has been transferred to the bottom plate which is of 18 mm stainless steel plate.

b) Provision to fix six targets and to change them without breaking the vacuum.

c) There are no restrictions in the number of detectors and their positions. They can be rotated together if desired , without breaking vacuum.

d) A gamma ray window for simultaneous measurement of γ-rays and charge particles.

e) A removable liquid nitrogen trap, which will reduce the carbon buildup on target, and which can be used to cool the Silicon detectors by means of leakage resistance, if desired.

f) Accurate and easy selection of angles and solid angles.

g) Easy lifting of top lid through controlled lever arrangements.

h) Fine control to adjust the chamber position along all the three axes for alignment.

8. <u>Beam Scanning System for Ion-implantation work</u> - N.S. Thampi and D.K. Sood - During ion-implantation work it is often necessary to sweep the ion-beam uniformly over a fixed area of the target. The PN 400 Van de Graaff Accelerator has a deflector system coupled to the extention tube for steering the beam. This consists of four 10 inches long 1 cm. dia stainless steel rods placed 90° apart on the circumference of a 3 cm dia circle and positioned inside a 3 inches dia aluminium tube by perspex holders. Electrical connections to the

deflector rods are brought out through glass-metal seals. Steering of the beam is achieved by applying appropriate voltage to one or both pairs of these rods. By using the same system and applying saw-tooth sweep voltages of different frequency to the two pairs of rods at 90°, a rectangular trace of the beam, of uniform intensity could be produced on a target.

The energy of the ion beam from the PN·400 accelerator is varied from 50 keV to 400 keV for different types of work. Also various kinds of ions are accelerated in the machine. To get a trace of 2 cm x 2 cm on a target with the present arrangements of auxiliary equipment, i.e. at a distance of about 1 foot from the deflector about 1.5 kV would be the maximum voltage requirement. Thus a sweep voltage variation of the order of 1 kV would meet the present requirement. This sweep voltage could be easily generated by modifying the existing H.T. supplies made by the Electronics Division. From figure 14 it can be seen that the H.T. output is taken across a condensor shunted by a potential divider chain of resistances. The last resistance of this chain which goes to ground is of 170 kΩ. The regulation of this supply is achieved by feeding the voltage across this resistance to the signal grid of a differential amplifier and associated control circuits. For modification to a saw-tooth sweep generator, this resistance was replaced by a 12 A x 7 tube, the plate of which was connected to the H.T. The capacitors in the output stage were disconnected. A standard saw-tooth generator was built using a 2021 tube. The saw tooth signal from this, after proper attenuation, was fed to the control grid of the 12 A x 7 tube. This makes the output voltage swing with the saw-tooth signal. The range of the sweep can be adjusted from 300-700 V at the lowest switch position to 500-1500V at the maximum of the switch. Two supplies were modified and sweep frequencies of 400 c/s and 40 kc/s were obtained.

By applying these voltages to the two sets of deflector rods at right angles a rectangular trace of the beam could be obtained on the target. Since the saw-tooth signal does not go to zero, the trace is not centred and undergoes a diagonal shift. By applying a compensating potential to the opposite rods, the trace could be brought back to centre. The system has been found quite satisfactory for producing a uniform sweep of ion-beam over a given area of the target.

ION IMPLANTATION STUDIES

1. Ion Implantation Facility - D.K. Sood, N.S. Thampi and N. Sarma - Ion implantation is a unique tool for injecting foreign atoms into solids to alter and control their electrical, electrochemical, mechanical, metallurgical, optical, magnetic and superconducting properties. A versatile ion implantation facility has been set up at Van de Graaff Laboratory for a study of these properties of solids.

A good ion implantation facility is required to possess the following features:

a) Well stabilized beams of almost all atomic species in the energy region of 10 to 500 keV
b) Analysing magnet with good mass separation capability
c) Magnetic/electrostatic focussing elements
d) X-Y scanning of beam to produce large uniform implanted layers
e) An efficient electron suppressor to minimise errors in beam current integration.
f) Implantation chamber to house the substrate
g) A two axis goniometer for channeled implantation or for post implantation channelling studies
h) Ultraclean vacuum system to produce vacuum better than 10^{-6} Torr
i) Conventional electronics for particle counting

The present ion implantation set up which meets most of the above mentioned requirements is shown schematically in Fig. 15.

The HVEC model PN 400 Van de Graaff accelerator is used for producing the ion beams. It has a 400 kV positive terminal with a rf ion source capable of delivering proton beam current upto 150 μA. This ion source has been found to give adequate currents of Xe^+ ($\sim 16 \mu$A), Kr^+ and N^+ ions. A gas manifold has been installed in the terminal to house two gas bottles either of which can be selected from the control panel. One of the bottles is filled with He to obtain alpha particles for analysing the implanted samples. A terminal voltage stabilizer has been fabricated and installed to get stability better than $\pm$ 0.5 kV at 400 kV.

A quadrupole lens has been fabricated and installed to focuss the beam to a small spot size ($\sim$1 mm diameter). An electrostatic system for X-Y scanning of beam has been fabricated. It consists of four stainless steel rods placed 90° apart across which saw-tooth voltage pulses are applied for X and Y scanning. Frequency of X deflecting voltage is 400 cps and that of Y deflecting voltage is 40000 cps. Pulse height can be varied from 300 to 1500 volts to adjust the range of scan.

With heavy ion beams, secondary electron emission from the Faraday cup region can be very copious; e.g. there may be as many as five secondary electrons per incident ion. Thus a rather efficient method is required for suppression of secondary electrons. We use a 180 volt battery for this purpose as shown in fig. 15. The negative electrode consists of a brass disc with a hole slightly larger than the target mask.

The substrate to be implanted, is mounted on a stainless steel flange which is bolted onto a six inch long brass tube. This tube is used as the Faraday cup. Alternately, a two axis goniometer can be used as the Faraday cup cum implantation chamber. Thus implantation along any predetermined axis of single crystal substrates is feasible.

A silicon surface barrier detector is mounted in the goniometer chamber at 150° to the beam direction. By using alpha particle beam (upto 400 keV), the ion implanted layers can be analysed by backscattering techniques. The output of the detector is fed to a conventional preamplifier amplifier system. One of the three pulse height analysers at the Van de Graaff Laboratory is then used for obtaining the spectra.

A three port analysing magnet has been designed for mass selection of the heavy ion beams. The maximum magnetic field of 6.5 k gauss would be adequate for bending He^{+} beam at 500 keV by 10°. Good mass separation upto mass number 132 would be available.

At present, we are limited to using only gas ions as the rf ion source accepts only gas charge. A versatile ion source capable of supplying ions of almost all atomic species is being acquired. Work is in progress on fabrication of a two axis goniometer, an implantation chamber and a muffle furnace (for post ion implantation annealing facilities). Orbitron ion pumps and sorption pumps are being installed to attain ultraclean high vacuum ($\lesssim 10^{-8}$ Torr).

2. Implantation and Recoil Implantation Studies - D.K. Sood and N.S. Thampi - Implantation of Xe^{+} and Kr^{+} ions into polycrystalline Al and single crystal Si have been carried out using the ion implantation set up described earlier. Recoil implantation of Cu into polycrystalline Al has been done using Kr^{+} and N^{+} ions. The recoil implantation technique has been used to make a thin p-n junction on an n-type Si crystal by recoil implanted Al dopant.

A pure polycrystalline Al sample was bombarded with 400 keV Xe^{+} ions to obtain a 1 cm diameter circular implanted layer. The fluence of Xe was 9×10^{16} ions/cm^2 as determined by the total integrated current. The implanted layer was then probed with 400, 300, 200 keV and 2 and 5 MeV alpha beams. Scattered alpha particles were detected in a detector mounted at 150° to the beam direction. Fig. 16 shows the spectrum for incident energy of 400 keV. The Xe peak, although merged with the contimuum arising from the thick Al substrate, is quite pronounced. In order to separate the Xe peak from the Al continuum, alpha particles of 5 MeV energy were used. Fig. 17 shows the spectrum obtained for a total charge of 5.72 μC of incident alphas. The various peaks were identified from kinematics.

The Xe peak is now well separated from the Al continuum. The sharp peak at 1.2 MeV is due to a thin carbon deposit on the substrate during implantation. To avoid cracking of carbon on the substrate, attempts were made to obtain cleaner and better vacuum. Liquid nitrogen traps at the forepump stages proved extremely useful in reducing backstreaming of oil vapour into system. This resulted in almost negligible carbon deposition as shown by the absence of carbon peak in the following results.

400 keV Xe^+ ions were then implanted in a well polished single crystal of Si cut normal to $\langle 111 \rangle$ axis. Total Xe^+ charge was 14712 μC. The 1 cm diameter implanted spot turned to a milky appearance due to radiation damage. The implanted crystal was probed with 2 MeV alpha particles. Fig. 18 (full curve) shows the scattered alpha spectrum. Xe peak is well separated from the Si continuum. Using the area under the Xe peak, the number n of Xe atoms/cm^2 can be obtained from the following equation.

$$n = 1.602 \times 10^{14} \frac{N}{\sigma q \Delta \Omega}$$

where σ is the Rutherford crosssection in mb, q is the total incident charge in μC, $\Delta\Omega$ is the solid angle in sterad and N is the total number of counts under the peak. Thus n is found to be 6.94×10^{16} ions/cm^2 which is in agreement with the fluence determined from the total Xe charge during implantation. This shows that the secondary electron suppression was very good, during beam charge measurements.

The implanted crystal was annealed in inert (Argon) atmosphere at 1000°C for 65 minutes. There was no change in the milky appearance of the implanted region showing persistance of radiation damage, inspite of anneal treatment. Another alpha spectrum, obtained after annealing the crystal, is shown as dashed curve in fig. 18. While there is no change in the Si continuum, Xe peak is much smaller. This shows thermal gas release of Xe during anneal treatment. From the areas under the Xe peaks, it is found that 20.3% of implanted Xe escapes during anneal treatment.

250 keV Kr^+ ions were implanted in another Si crystal to a fluence of 6.24×10^{14} ions/cm^2. The 2 MeV alpha scattering spectrum is shown in fig. 19. The total alpha charge of 28.58μC had to be put to obtain this rather small peak of Kr. The small yield is due to much smaller dose of Kr and much smaller Rutherford cross-section.

If a thin film of a material is deposited on the substrate prior to ion bombardment, the atoms of the thin film material get implanted in the substrate lattice by virtue of their recoil energy. This phenomenon of recoil implantation could turn out to be an efficient tool for implantation of metallic ions using gas ion beams. As it is more convenient and more economic to produce and handle gas ion beams, the recoil implantation technique is likely to find several industrial applications requiring metallic-ion implantation. We have, therefore, started on a research program to study the characteristics of this technique. The program is aimed at the study of the number β, of recoil implanted atoms per incident gas ion, the variation of β with incident ion dose, energy, charge and mass, and of the depth profile of the recoil implanted atoms. Some of the preliminary results obtained so far are described below:

Thin films of copper (ranging from 37 gm/cm^2 to 112 gm/cm^2) were vacuum-evaporated on polycrystalline aluminium foil samples. N^+ and Kr^+ ions of 300 keV energy were implanted uniformly over a circular area of one cm. diameter on these samples, to fluences$\sim 10^{13}$/cm^2 to 10^{15}/cm^2.

Nitric acid is quite suitable for removal of evaporated copper which is dissolved readily whereas aluminium is not attacked by it.

When the implanted samples were immersed in 20% nitric acid, it was found that the chemical reaction rate is reduced considerably in the implanted region. Whereas copper in the unimplanted region of the sample was removed in about 10 minutes, the implanted region was covered with copper even after two hours of acid treatment. This was a major experimental difficulty in getting quantitative results on β. Some of the qualitative results are shown in fig. 20 which shows spectra of 2 MeV alpha particle scattering (observed at 150°) from two such samples bombarded with 5×10^{14} ions/cm^2 of 300 keV Kr^+ (full circles) and N^+ (open circles) ions. Post implantation treatment of the 112 μgm/cm^2 thin film of copper (about three times the range of 300 keV Kr^+) was done in 60% nitric acid for one hour. This time was probably long enough to remove all the unimplanted copper. The peak at channel number 74 is due to recoil implanted copper. Similar spectra obtained after scattering from the unimplanted region of the samples do not show any such peak, indicating complete removal of copper under acid treatment. The copper peak due to Kr^+ ions is much stronger. From fig. 20 we find that

$$\frac{\beta_{Kr^+}}{\beta_{N^+}} = 8.23$$

These results are in qualitative agreement with the theory of Nelson[1] which predicts a ratio of 13.

The technique of recoil implantation has been used successfuly to dope Al atoms in an n-type Si crystal. As Al is p-type, we get a thin p-n junction in Si.

An Al film of thickness $\sim$100 μgm/cm^2 (which is just greater than the range of 200 keV N^+ ions in Al) was vacuum evaporated on freshly etched n-type Si crystal of 2 cm diameter and resistivity of 10,000 ohm cm. It was then bombarded uniformly with 200 keV N^+ ions through a circular mask of 1 cm diameter. The fluence of N^+ ions was $10^{15}/cm^2$. Aluminium film was removed using concentrated Hcl bath for one hour. In order to heal the radiation damage, the crystal was annealed in Argon atmosphere at 700°C for 35 minutes. It has already been shown[2] that these anneal conditions are optimum for obtaining the largest carrier concentration.

The analysis of the recoil implanted layer was done with a hot probe which indicates that the layer is strongly p-type. Thus a p-n junction has been formed. The experiments are in progress to determine the junction characteristics.

1) R.S. Nelson, Radiation Effects 2(1969)47

2) J.W. Mayer, L. Eriksson and J.A. Davies, 'Ion Implantation in Semiconductors', Academic Press, 1970, page 183.

3. Radiation Damage in Si Implanted with Kr^+ Ions - D.K. Sood and N.S. Thampi - Channeling-effect measurements have been used extensively[1-3] to obtain a quantitative measure of the amount of disorder in ion-implanted single crystals. We have used this method to study the fluence dependence of the amount of disorder produced in <111> Si by implantation of 200 keV Kr^+ ions.

An optical grade polished crystal of Si cut approximately normal to <111> axis was chosen for this purpose. The crystal was mounted on a two axis goniometer and backscattering of 2 MeV alpha particle beam was used for alignment. The channeling dip, shown in fig. 21 occurs at $\theta = -2.4°$ and $\phi = 75°$. It may be seen that 95% of the incident particles are channeled. The FWHM is equal to 0.96°, corresponding to a critical angle of 0.48°. The random and aligned spectra obtained at $\theta = 8°$ and $-2.4°$ are shown in fig. 22. The energy of the scattered particles is a measure of the depth of the scattering event. The larger is the depth of penetration, the smaller is the energy of scattering. Therefore, the scattered particles observed around the largest channel numbers in fig. 22 correspond to those scattered from the proximity of the crystal surface. The aligned spectrum (open circles) falls of monotonously at higher channel numbers. This indicates that the crystal is good and is free from any disorder in the lattice; since the atoms displaced by more than about 0.15Å from the lattice sites would contribute to random scattering and cause a surface peak in the aligned spectrum.

The crystal was then implanted with 200 keV Kr^+ ions, through a circular mask of 1 cm. diameter, successively in three steps to obtain fluence of 1, 2 and 4 micro Coulombs/cm^2. (One micro Coulomb/cm^2 = 6.242×10^{12} ions/cm^2). After each implantation step, the crystal was mounted on the goniometer and 2 MeV alpha beam was used to obtain the channeled spectrum. Figure 23 shows four channeled spectra corresponding to fluences of 0, 1, 2 and 4 μC. The surface damage peak starts appearing at 1 μC and increases in intensity with increasing fluence. Using the area under the damaged peak, corrected for dechanneling background, and the Rutherford cross-section we get the number of displaced silicon atoms as $1.062 \times 10^{17}/cm^2$. For influence of 4 μC (corresponding to 2.497×10^{13} Kr^+ ions/cm^2) the number of the displaced lattice (silicon) atoms per incident Kr ion is found to be 4253. This is quite high disorder and is in qualitative agreement with the theoretical estimate of Kinchin and Pease[4].

Experiments are in progress to observe damage at higher fluences, to determine the energy dependence of η and to study the anneal behaviour of the damage.

1) E. Bogh, Can. J. Phys. 46(1968)653

2) J.A. Davies, J. Denhertog, L. Eriksson and J.W. Mayer, Can. J. Phys. 45(1967)4053

3) D.A. Marsden, G.R. Bellavance, J.A. Davies, M. Martini and P. Sigmund, Phys. Stat. Sol. 35(1969)269

4) G.H. Kinchin and R.S. Pease, Rept. Prog. Phys. 18(1955)1

4. <u>A New Plastic Detector</u> - D.K. Sood - Charged particles traversing an insulating medium leave a radiation damage trail which can, often, be selectively attacked by a suitable chemical reagent to produce tracks visible under an optical microscope. Several solid state track detectors such as mica, glasses and plastics have been developed and used extensively. Each detector is characterised by a critical energy loss rate $(dE/dx)_{crit.}$ below which no tracks are registered. Thus most of the detectors proposed so far could record ions heavier than α-particles. We have developed a new plastic (Cellulose triacetate) detector capable of registering protons of energy as low as 50 keV. The response of this detector to 400, 300, 200, 100 and 50 keV protons; 5.48 MeV, 400 and 200 keV alphas; 300 keV N^+ ions and 300 keV Kr^+ ions has been studied. The diameter of the tracks is found to increase with etching time (6N NaOH at 60°C) and with dE/dx of the incident particle. It is shown that the detector possesses rather good particle identification characteristics which make it suitable for a wide range of applications in nuclear physics, solid state physics and astrophysics.

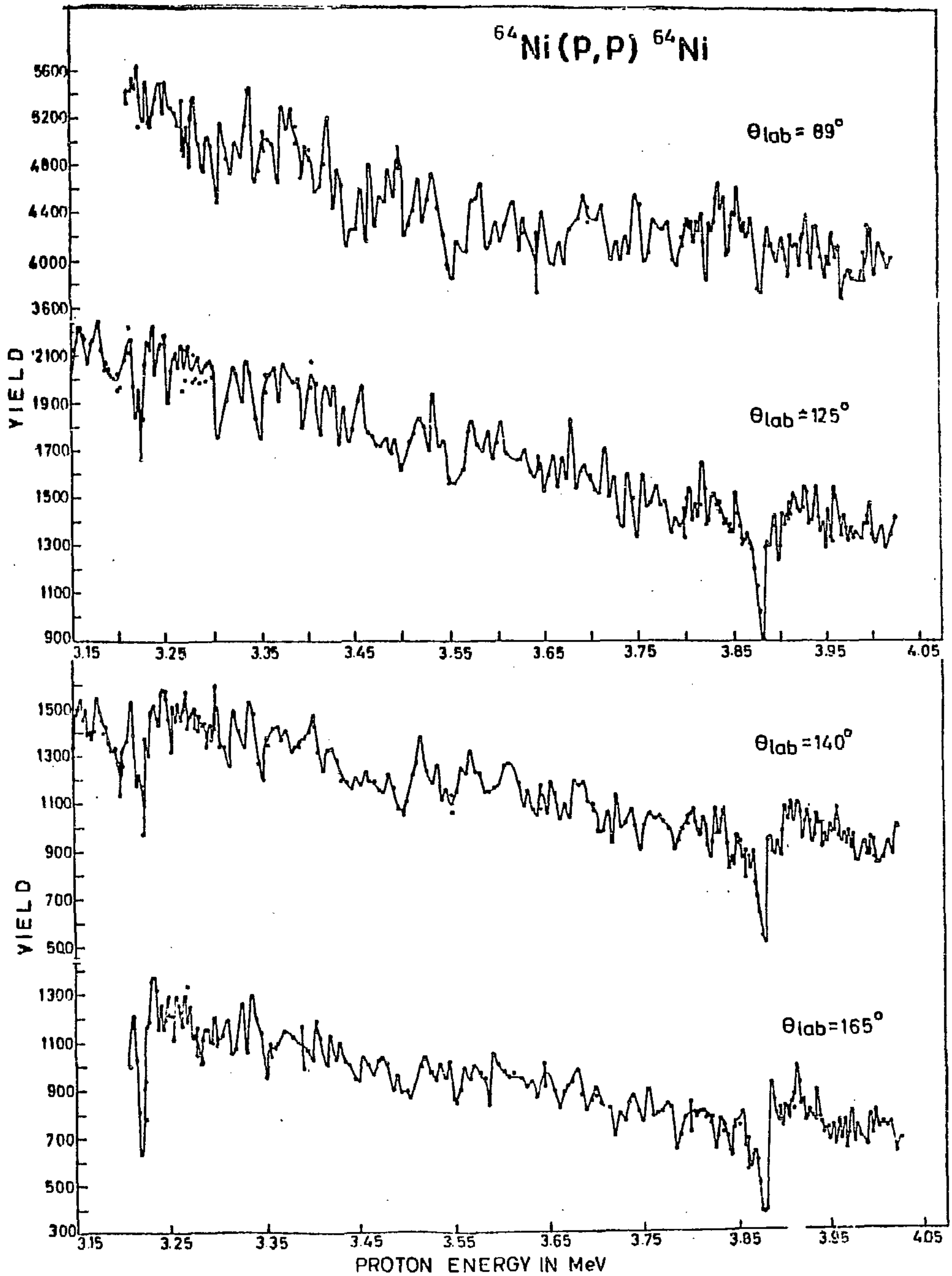

$^{64}Ni(P,P)\,^{64}Ni$
$\theta_{lab} = 89°$
$\theta_{lab} = 125°$
$\theta_{lab} = 140°$
$\theta_{lab} = 165°$
YIELD
YIELD
PROTON ENERGY IN MeV

FIG.1

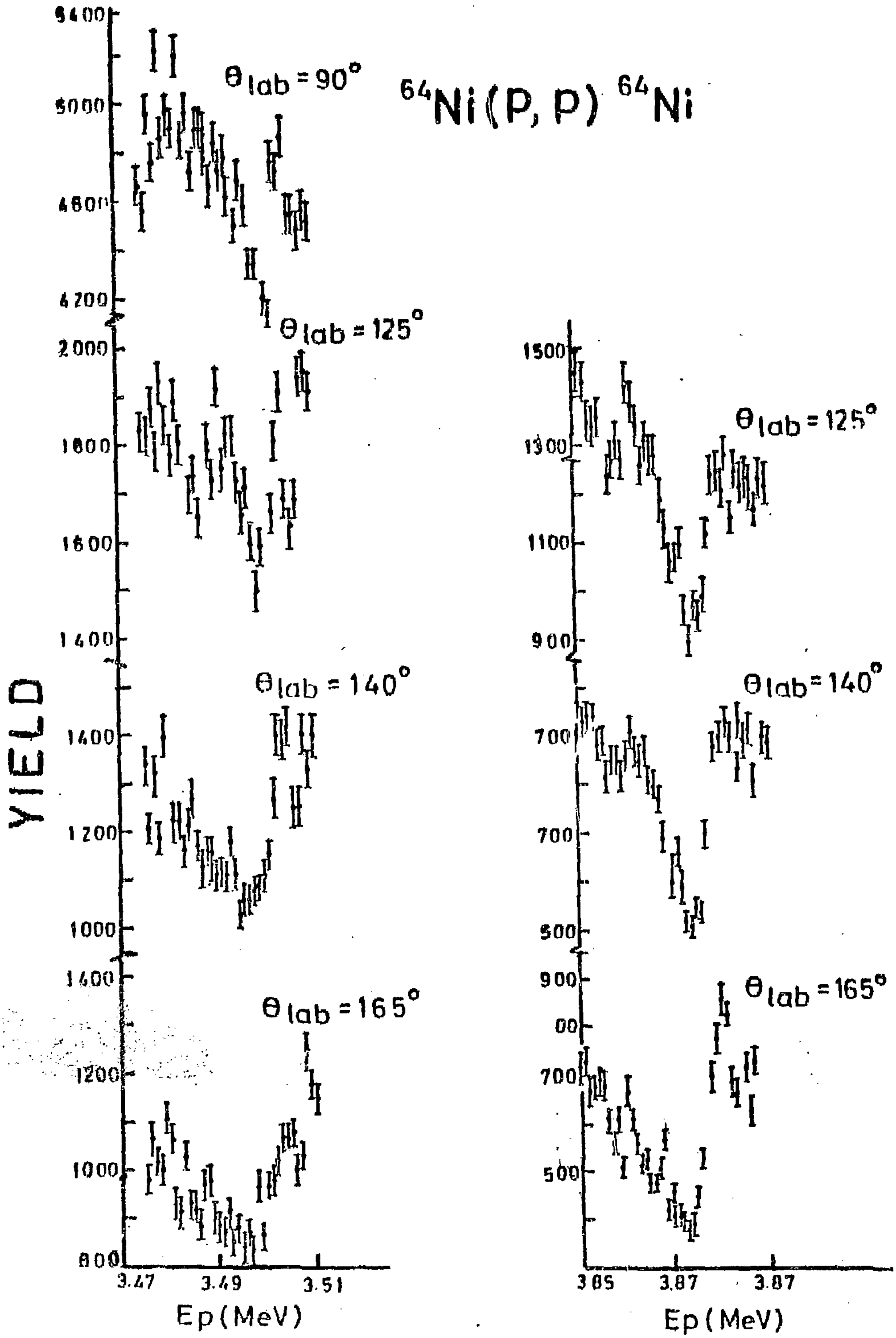

FIG. 2

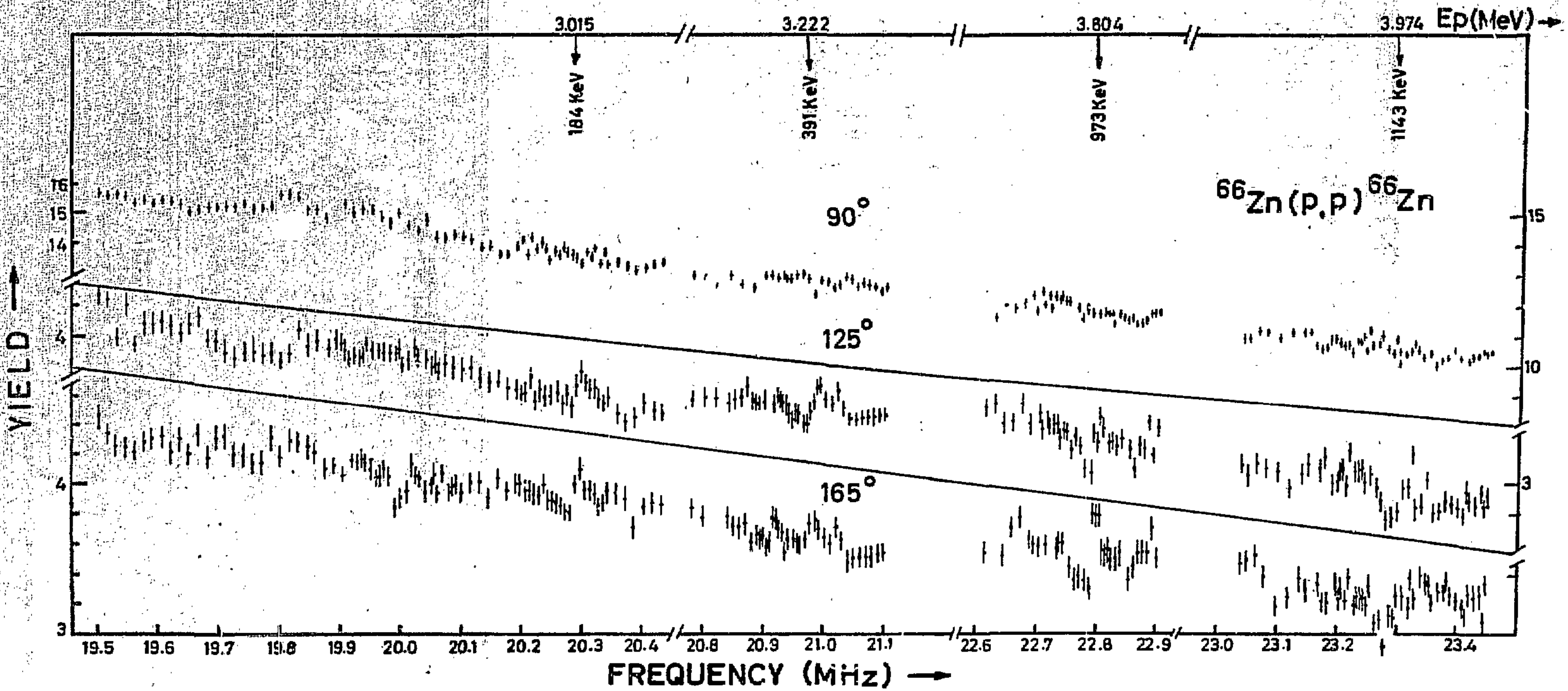

3.015
3.222
3.804
3.974
Ep(MeV)
184 KeV
391 KeV
973 KeV
1143 KeV
$^{66}Zn(p,p)^{66}Zn$
90°
125°
165°
YIELD
16
15
14
4
4
3
15
10
3
19.5
19.6
19.7
19.8
19.9
20.0
20.1
20.2
20.3
20.4
20.8
20.9
21.0
21.1
22.6
22.7
22.8
22.9
23.0
23.1
23.2
23.4
FREQUENCY (MHz)

FIG. 3

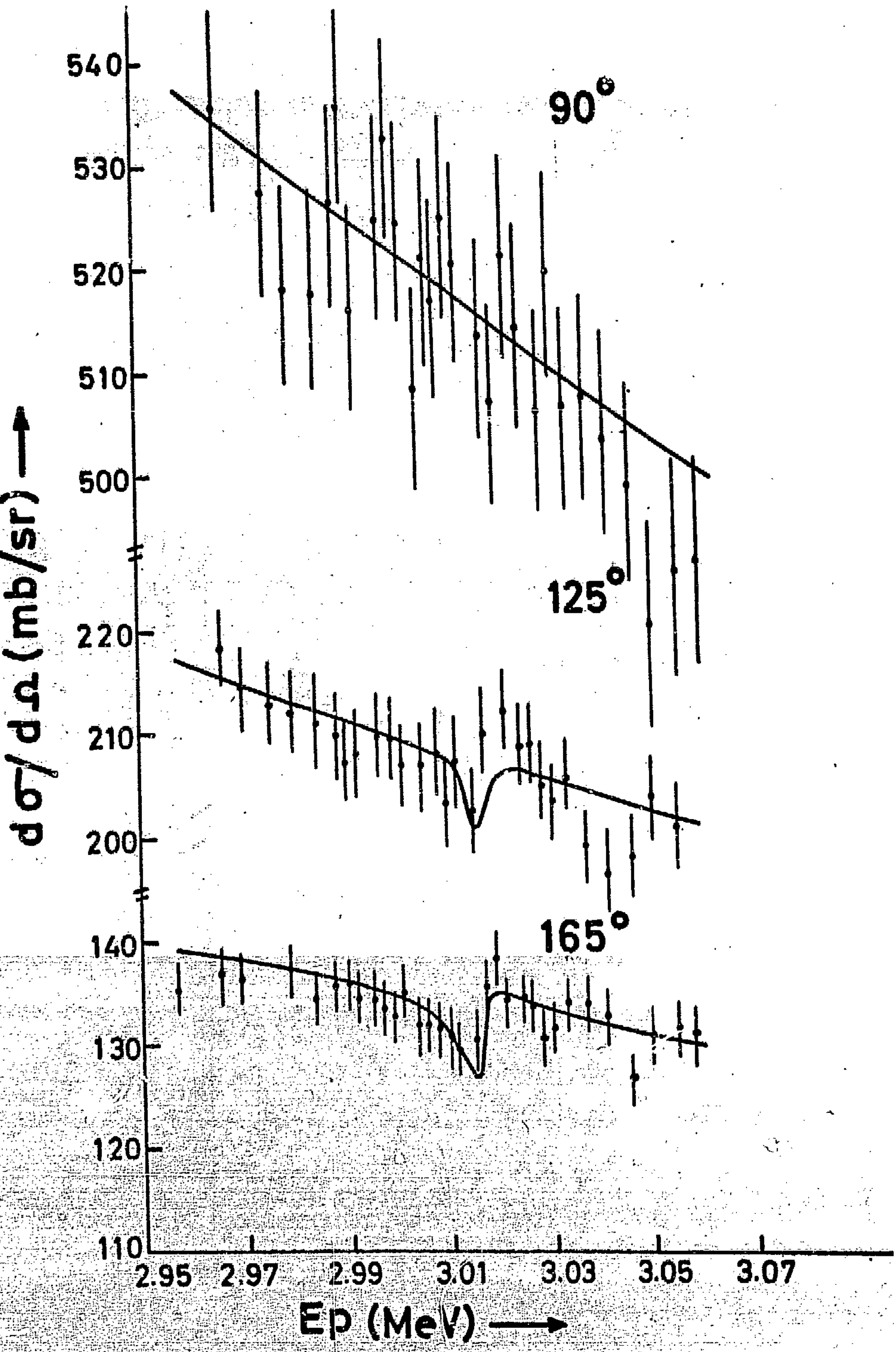
540
530
520
510
500
220
210
200
140
130
120
110
90°
125°
165°
dσ/dΩ (mb/sr) →
2.95
2.97
2.99
3.01
3.03
3.05
3.07
Ep (MeV) →

FIG.4a

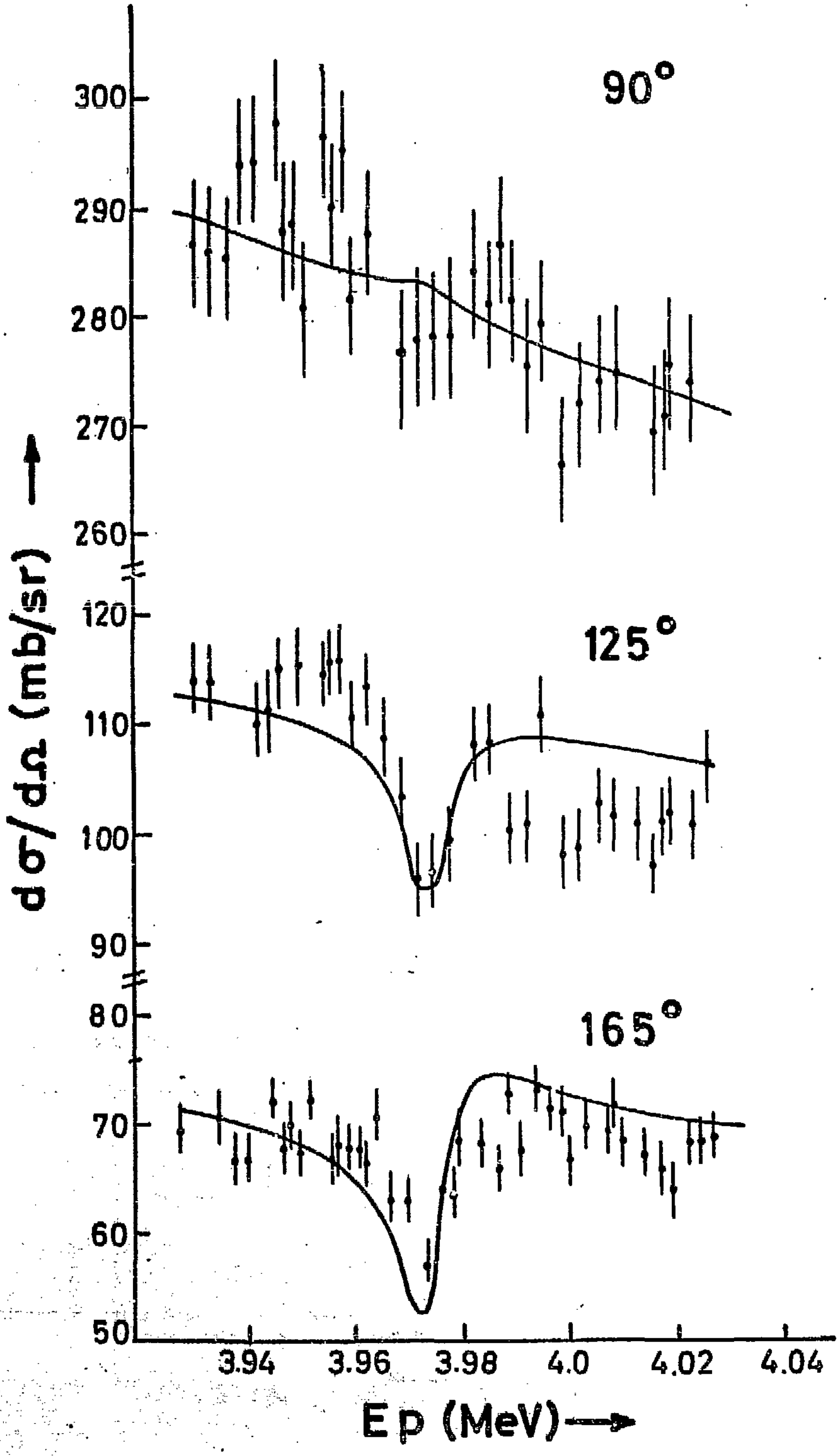
90°
125°
165°
300
290
280
270
260
120
110
100
90
80
70
60
50
dσ/dΩ (mb/sr)
3.94
3.96
3.98
4.0
4.02
4.04
Ep (MeV)

FIG.4c

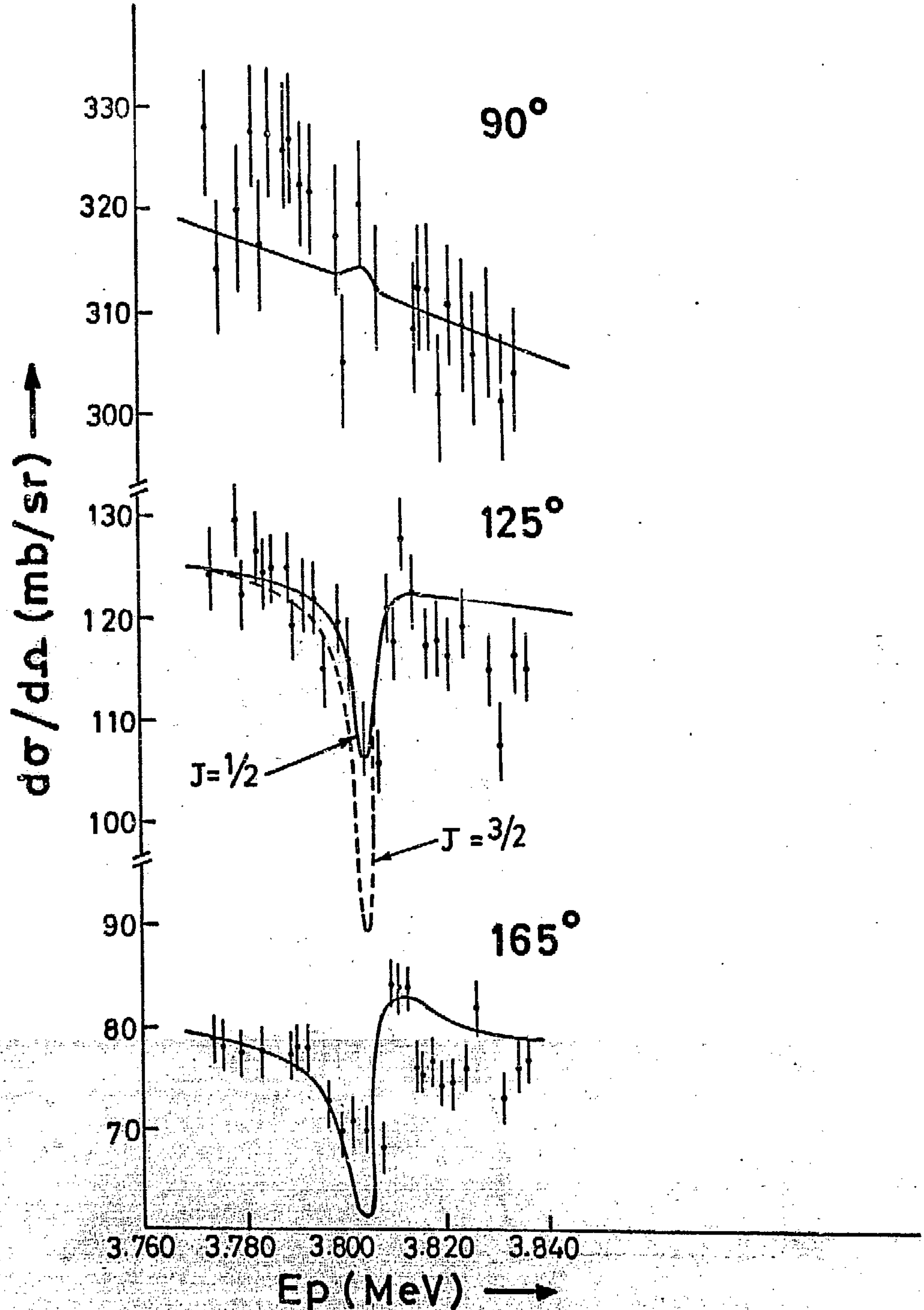

330
320
310
300
130
120
110
100
90
80
70
90°
125°
165°
J=1/2
J =3/2
dσ/dΩ (mb/sr)
3.760
3.780
3.800
3.820
3.840
Ep (MeV)

FIG. 4b

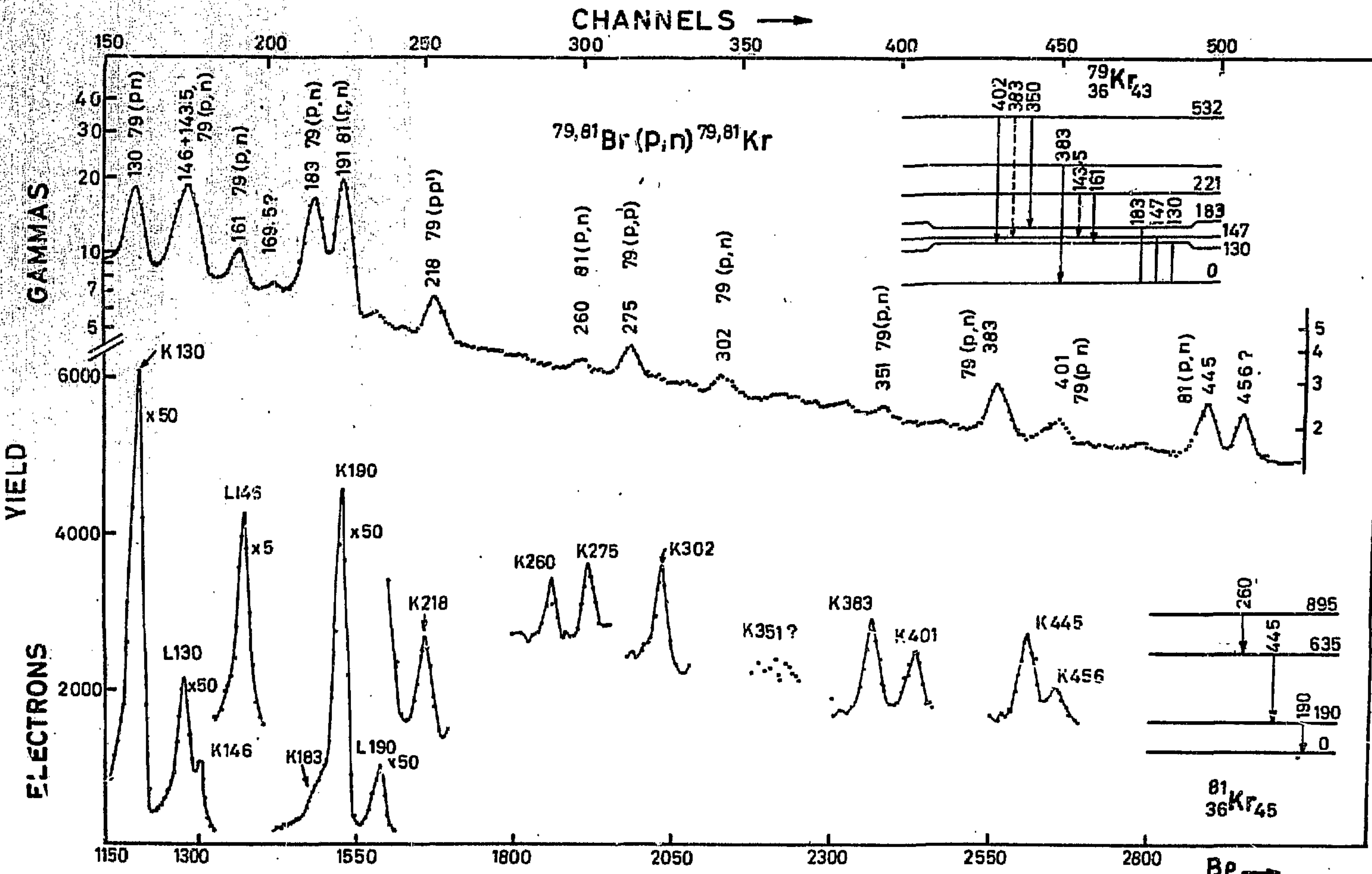
CHANNELS
$^{79,81}Br(p,n)^{79,81}Kr$
$^{79}_{36}Kr_{43}$
$^{81}_{36}Kr_{45}$
GAMMAS
YIELD
ELECTRONS
Bρ
K130
L130
K146
L146
K183
K190
L190
K218
K260
K275
K302
K351 ?
K383
K401
K445
K456

FIG. 5

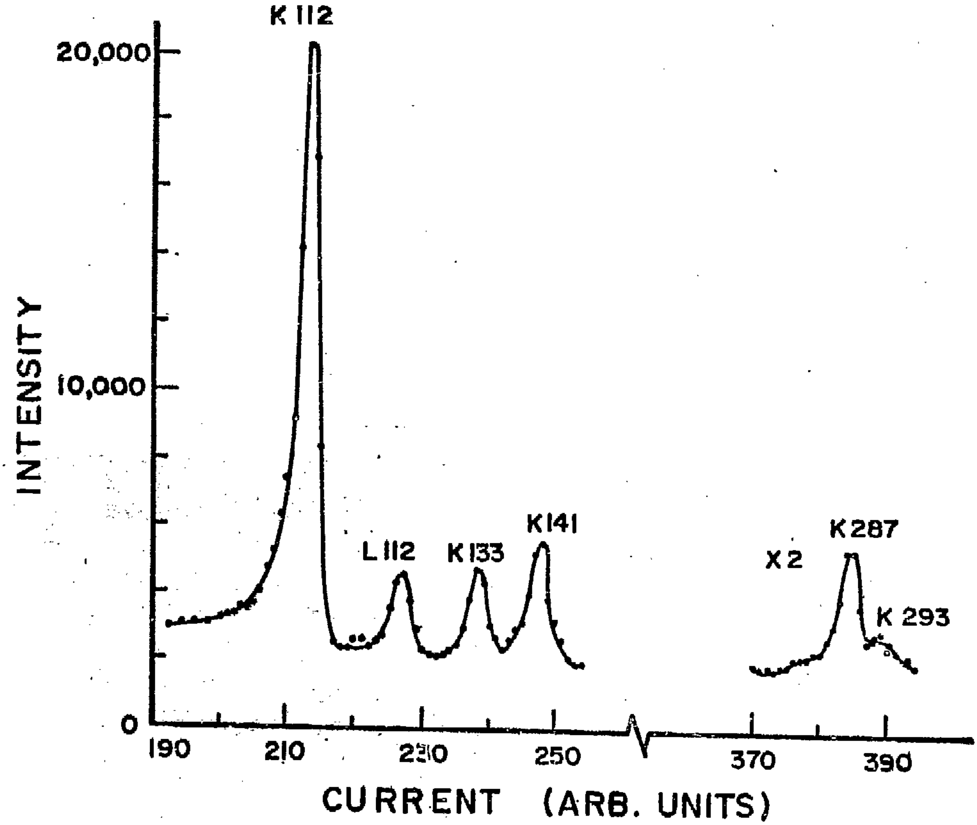
K 112
20,000
10,000
0
INTENSITY
L 112
K 133
K 141
X 2
K 287
K 293
190
210
230
250
370
390
CURRENT (ARB. UNITS)

FIG - 6

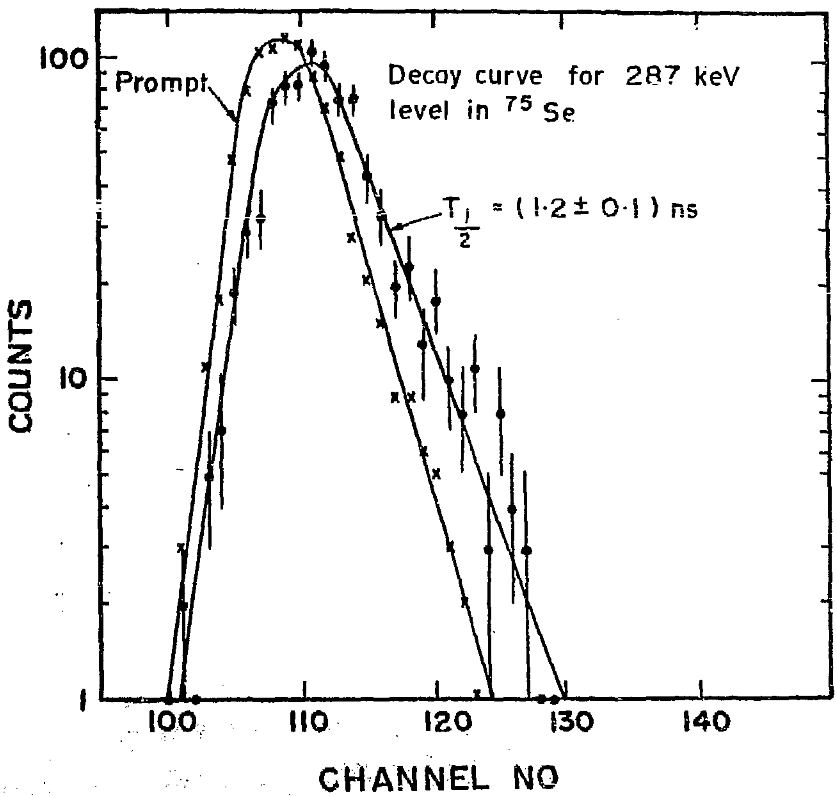

Decay curve for 287 keV
level in 75 Se
Prompt
$T_{\frac{1}{2}} = (1{\cdot}2 \pm 0{\cdot}1)$ ns
COUNTS
100
10
1
100
110
120
130
140
CHANNEL NO

FIG.7

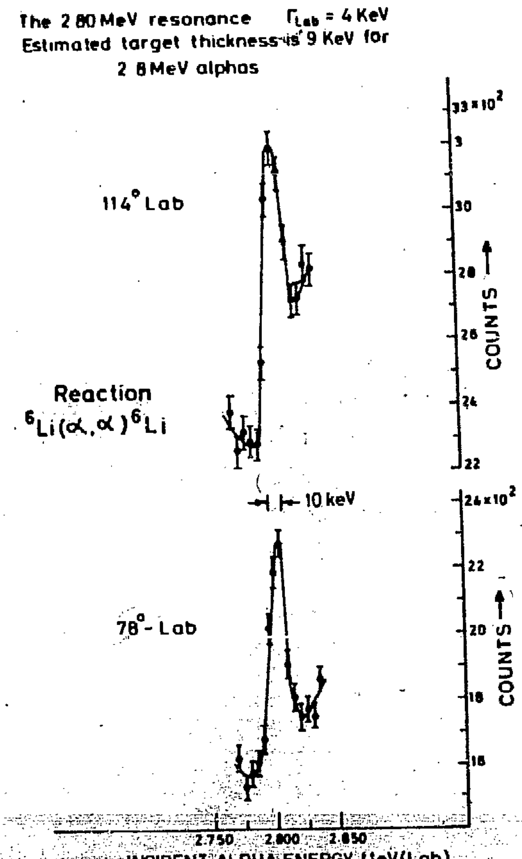
The 2.80 MeV resonance Γ Lab = 4 KeV
Estimated target thickness is 9 KeV for
2.8 MeV alphas
114° Lab
Reaction
6Li(α,α)6Li
10 keV
78°- Lab
COUNTS
COUNTS
2.750
2.800
2.850
INCIDENT ALPHA ENERGY, MeV(Lab)

FIG. 8

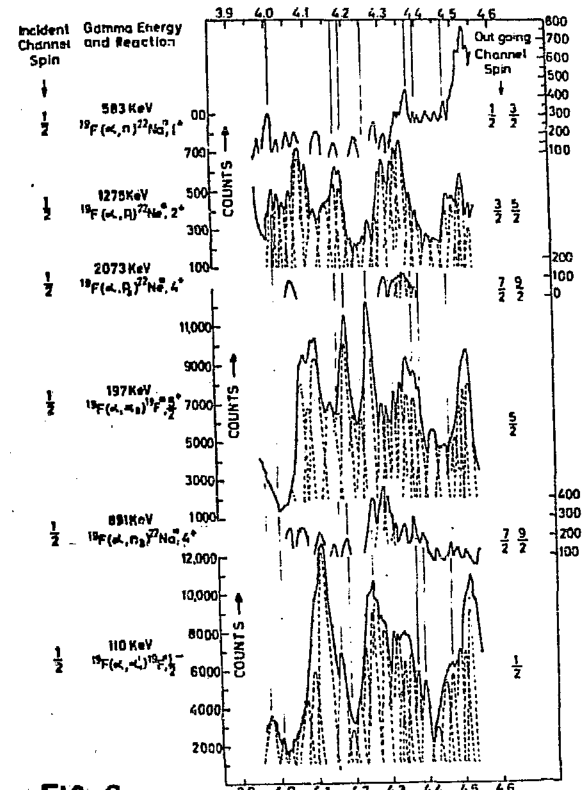

FIG. 9

FIG. 2 INCIDENT ALPHA ENERGY, MeV (Lab) →
YIELD OF GAMMARAYS AT DIFFERENT CHANNELS

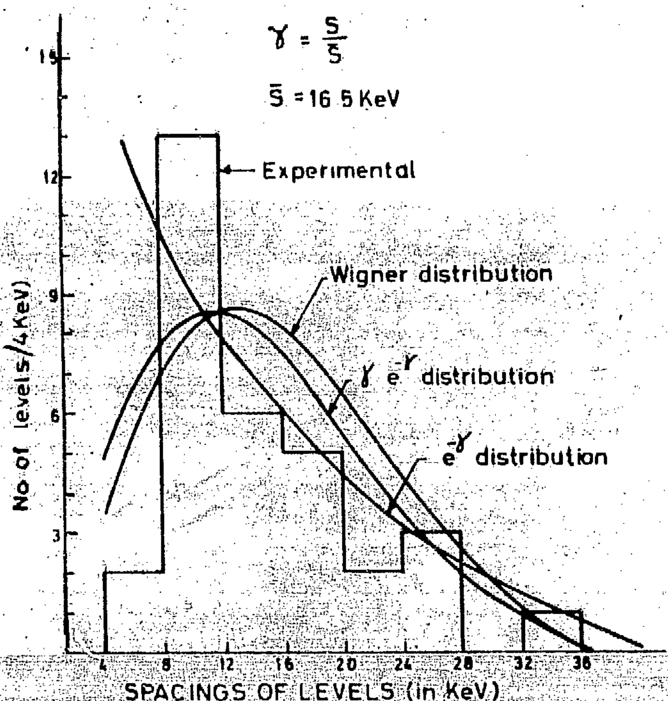

$\gamma = \frac{S}{\bar{S}}$
$\bar{S} = 16.5$ KeV
Experimental
Wigner distribution
$\gamma e^{-\gamma}$ distribution
$e^{-\gamma}$ distribution
No of levels/4 KeV
15
12
9
6
3
4
8
12
16
20
24
28
32
36
SPACINGS OF LEVELS (in KeV)

FIG. 10

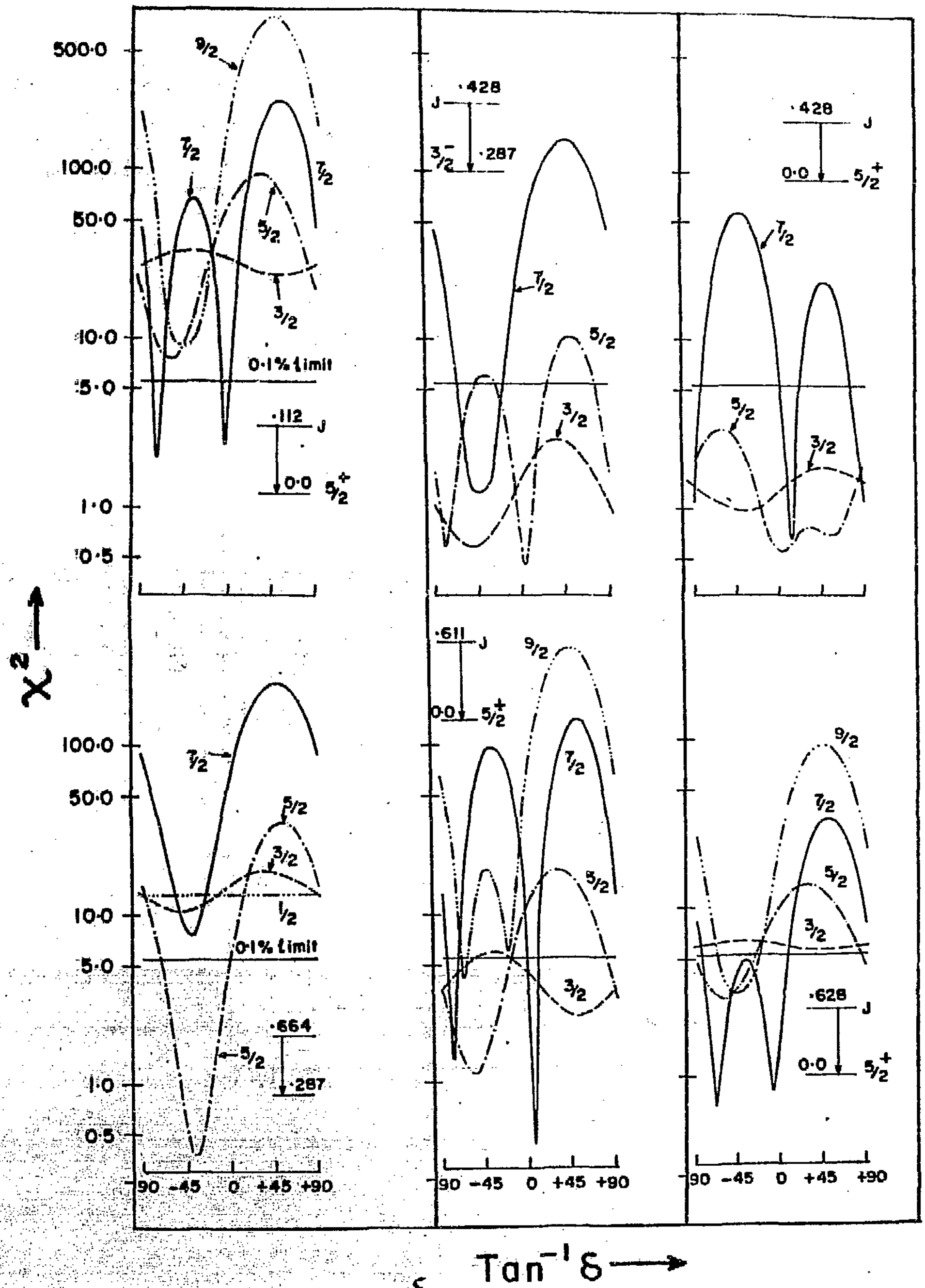

FIG.2. χ^2 vs tan$^{-1}\delta$ plots for the angular distributions studied. 0.1% confidence limit is shown in each plot.

FIG.11

NEUTRON TIME-OF-FLIGHT SET UP USING ASSOCIATED γ-RAY

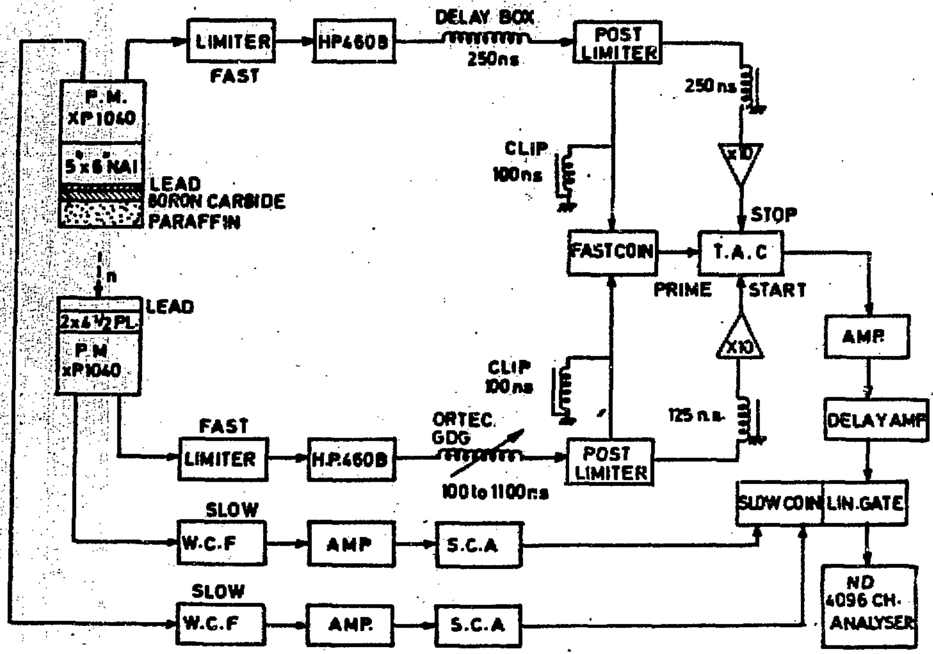

FIG.12

NEUTRON TIME OF FLIGHT SPECTRA FROM Am-Be SOURCE WITH n-γ COINCIDENCES

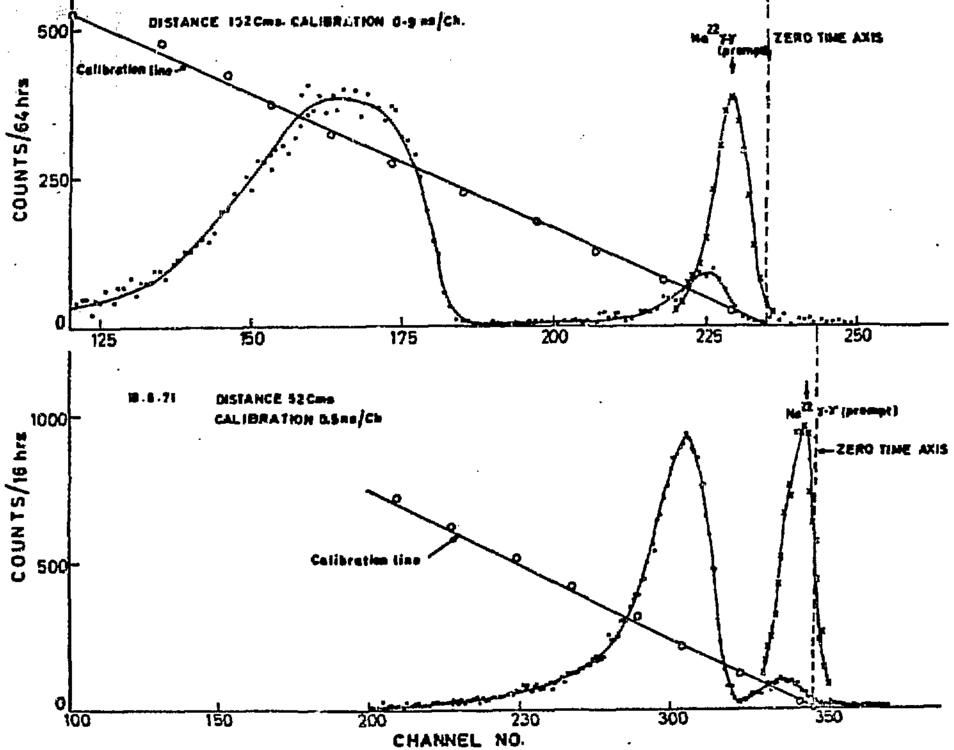

FIG. 13

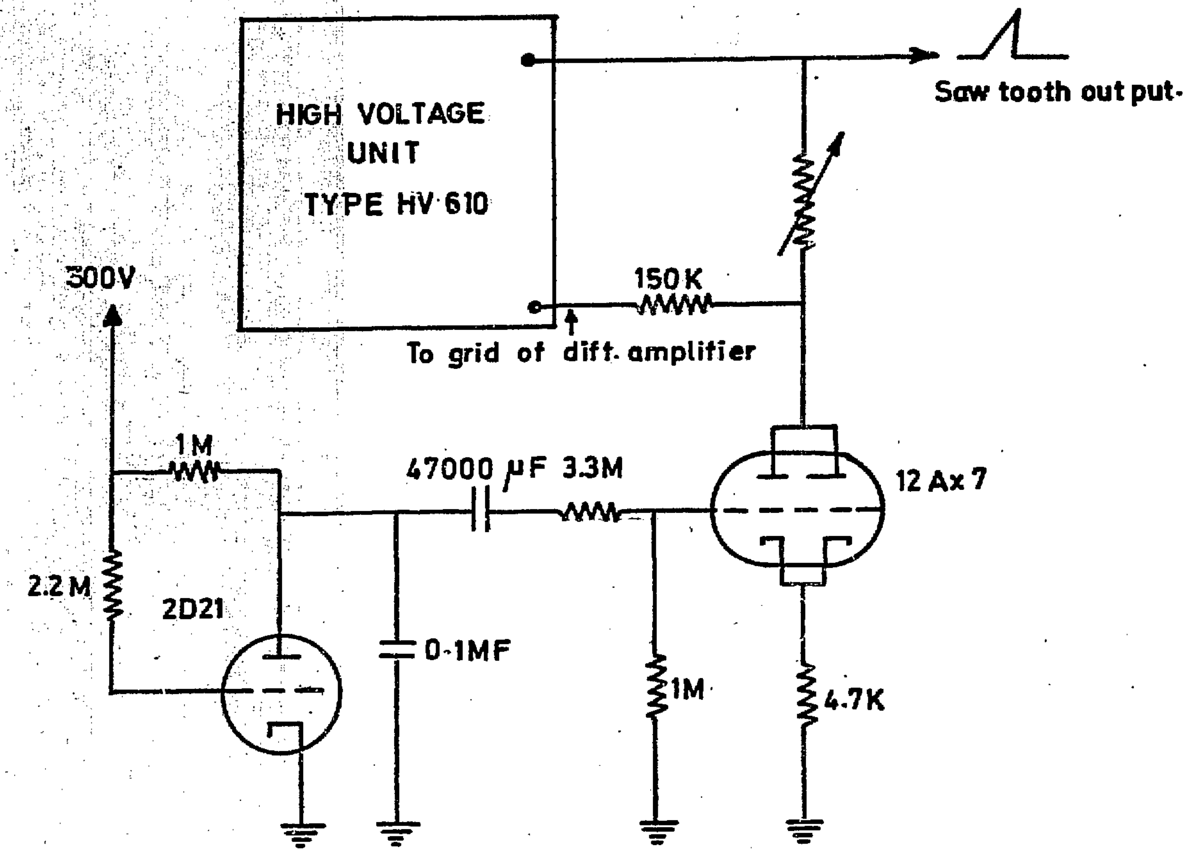

HIGH VOLTAGE UNIT TYPE HV 610
Saw tooth out put-
150K
To grid of dift. amplifier
300V
1M
47000 µF
3.3M
12 Ax 7
2.2 M
2D21
0·1MF
1M
4.7K

FIG.14

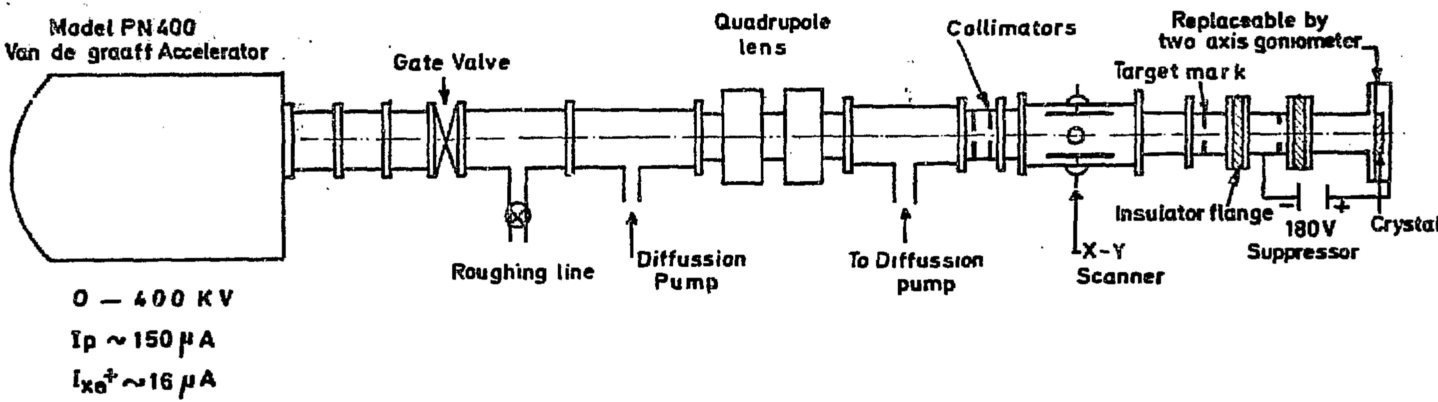
Model PN 400
Van de graaff Accelerator
Gate Valve
Quadrupole lens
Collimators
Replaceable by two axis goniometer
Target mark
Roughing line
Diffussion Pump
To Diffussion pump
X-Y Scanner
Insulator flange
180 V
Suppressor
Crystal
0 — 400 KV
Ip ~ 150 μA
I_{Xe^+} ~ 16 μA

FIG.15

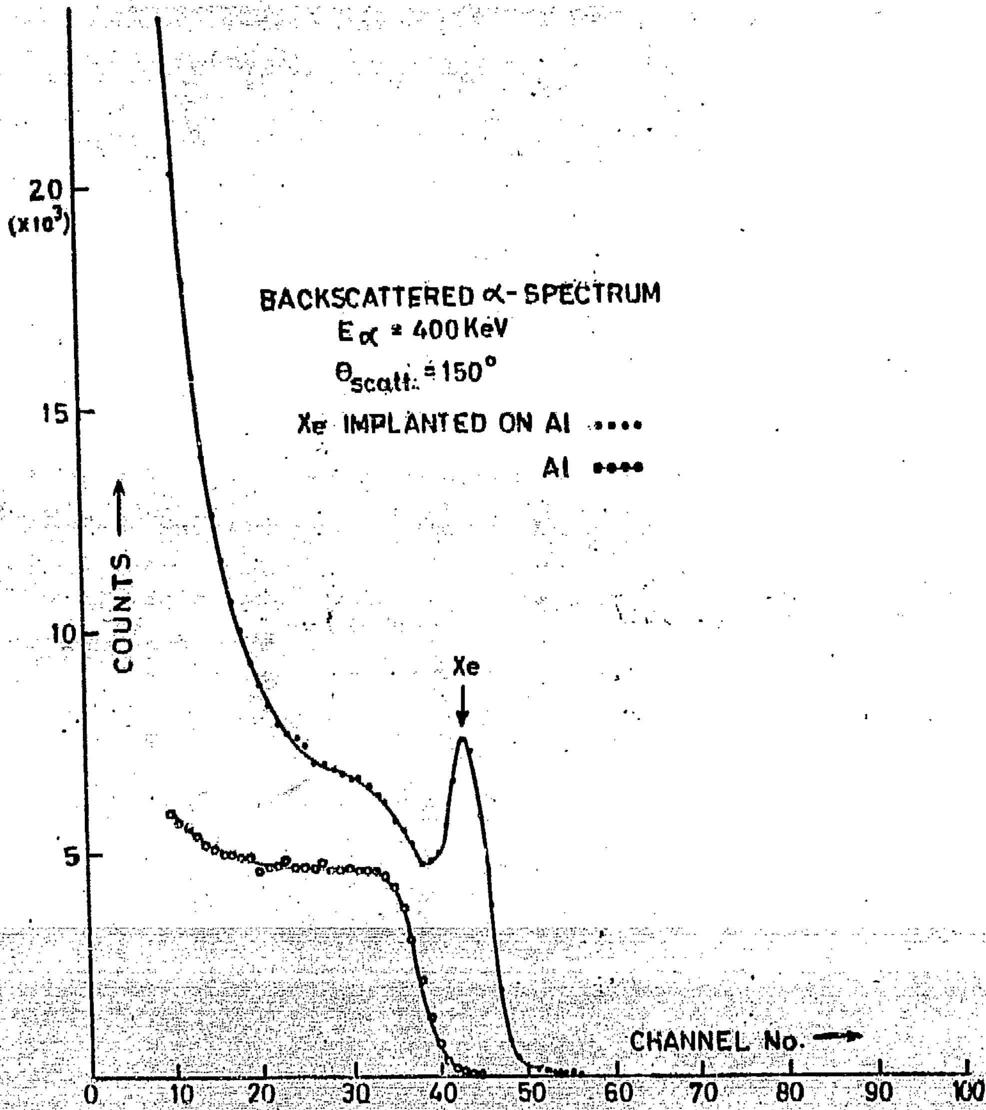

20
(x10³)
15
10
5
COUNTS
BACKSCATTERED α- SPECTRUM
Eα = 400 KeV
θscatt. = 150°
Xe IMPLANTED ON Al
Al
Xe
CHANNEL No.
0
10
20
30
40
50
60
70
80
90
100

FIG.16

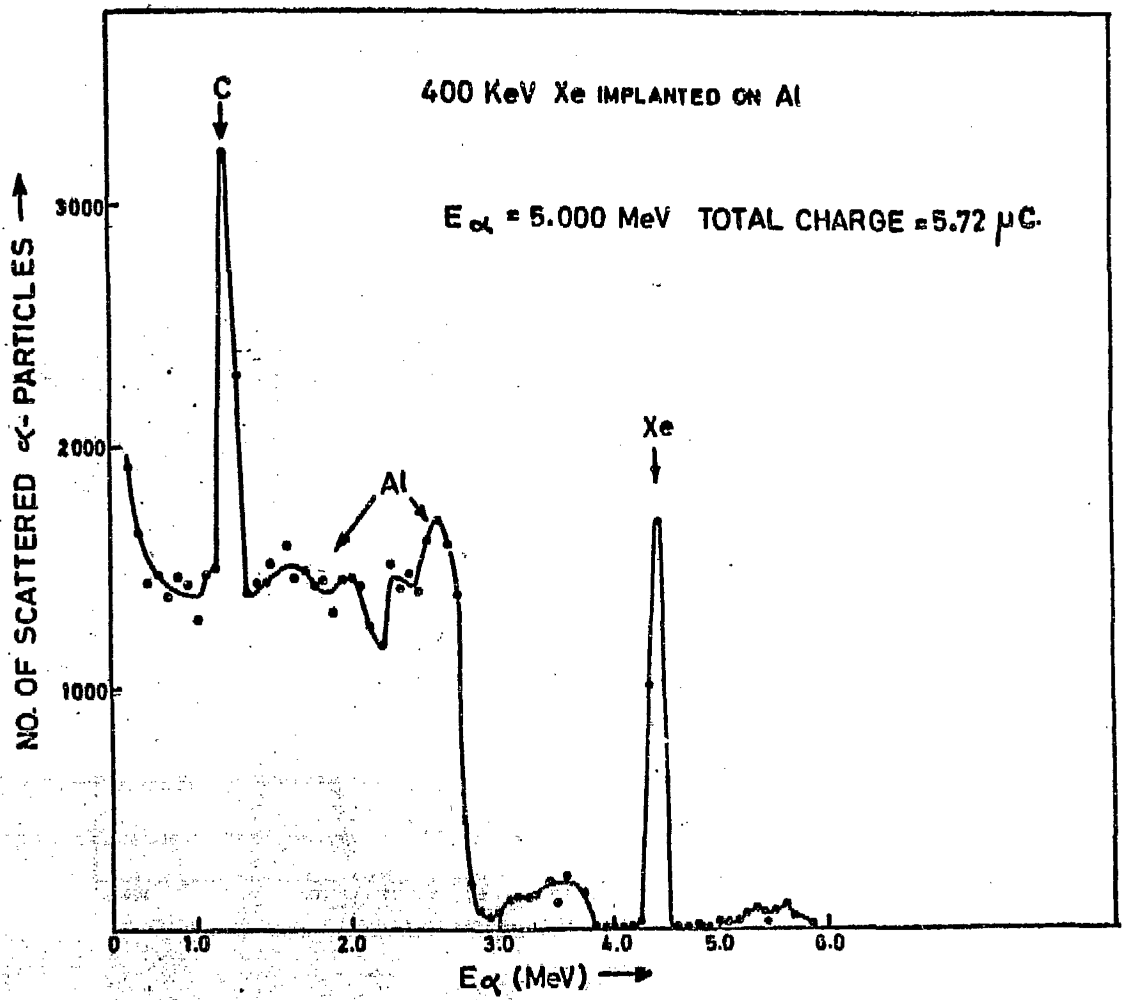

400 KeV Xe IMPLANTED ON Al
E α = 5.000 MeV TOTAL CHARGE = 5.72 μC
C
Al
Xe
NO. OF SCATTERED α- PARTICLES
3000
2000
1000
0
1.0
2.0
3.0
4.0
5.0
6.0
Eα (MeV)

FIG.17

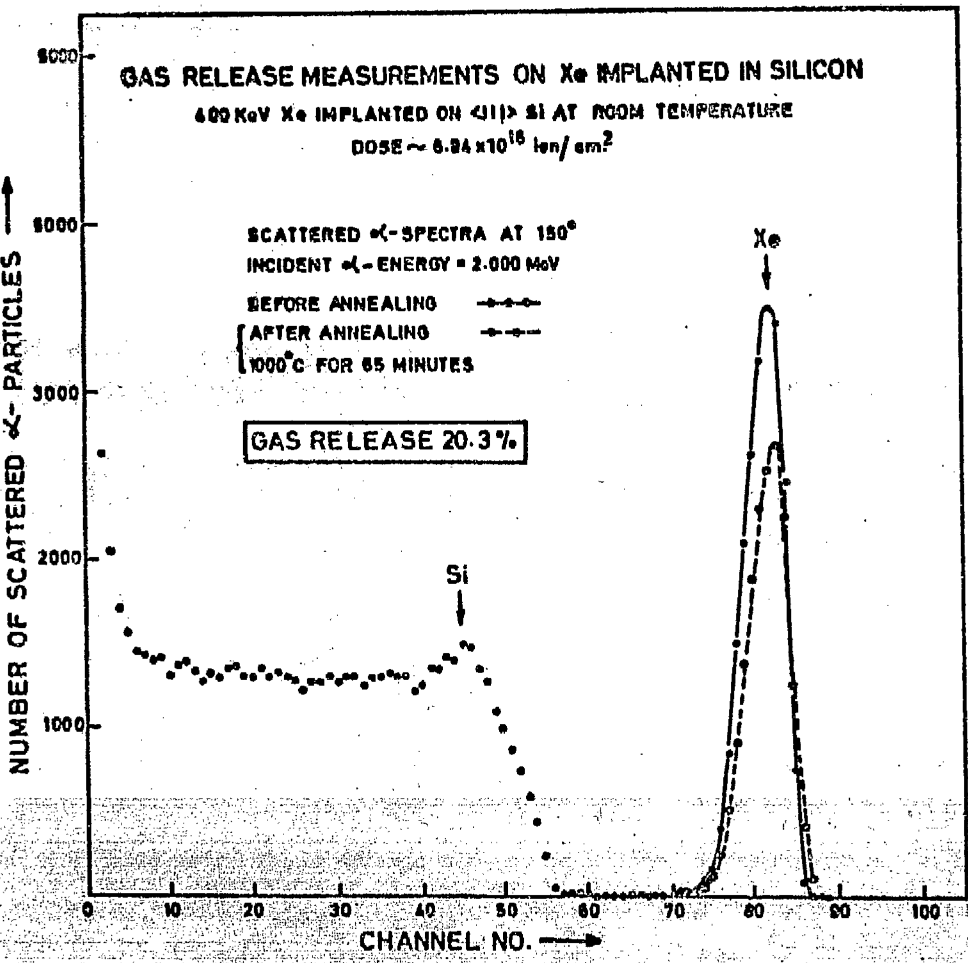

GAS RELEASE MEASUREMENTS ON Xe IMPLANTED IN SILICON
600 KeV Xe IMPLANTED ON <111> Si AT ROOM TEMPERATURE
DOSE ~ 6.94 x 10^16 ion/cm^2
SCATTERED α-SPECTRA AT 150°
INCIDENT α-ENERGY = 2.000 MeV
BEFORE ANNEALING
AFTER ANNEALING
1000°C FOR 65 MINUTES
GAS RELEASE 20.3%
Xe
Si
NUMBER OF SCATTERED α- PARTICLES
CHANNEL NO.

FIG.18

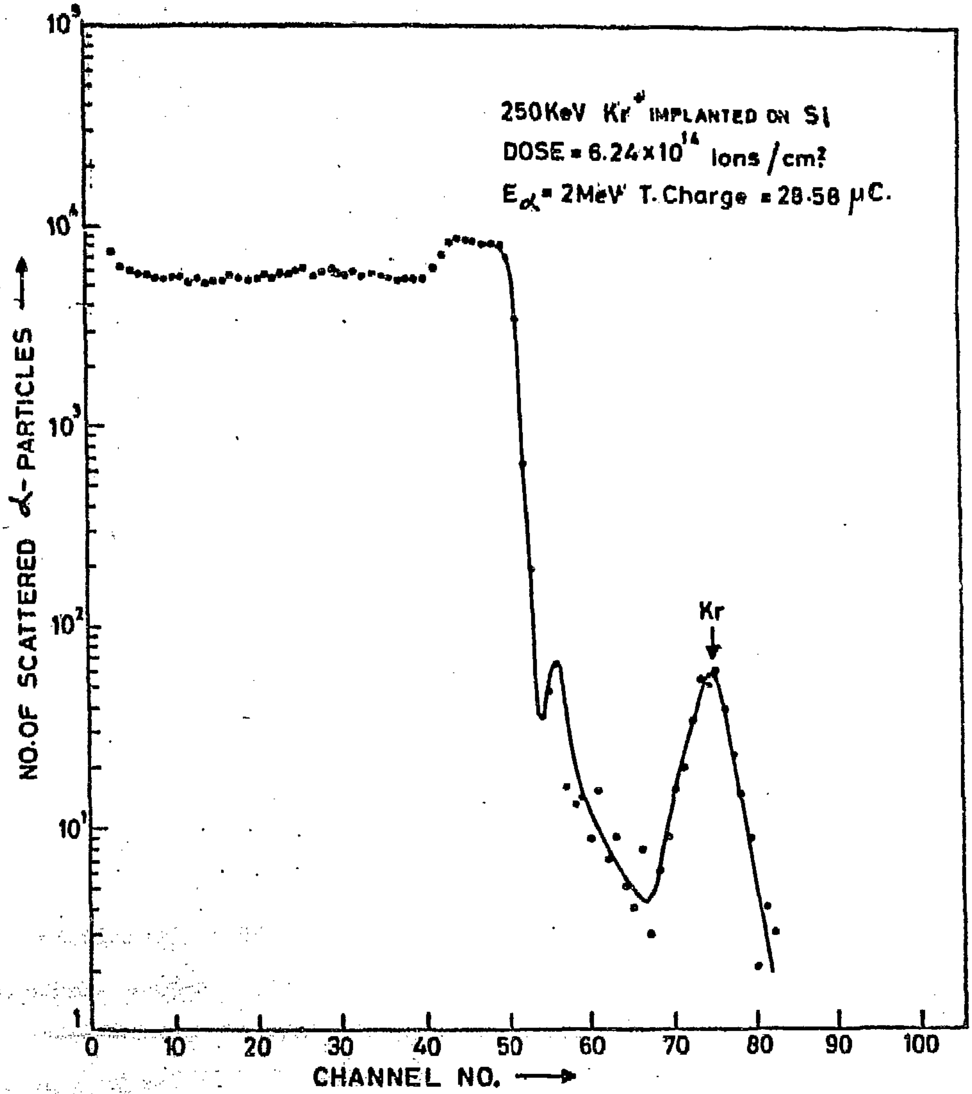

250KeV Kr+ IMPLANTED ON Si
DOSE = 6.24x10^14 Ions/cm²
Eα = 2MeV T.Charge = 28.58 μC.
Kr
NO.OF SCATTERED α- PARTICLES
CHANNEL NO.

FIG.19

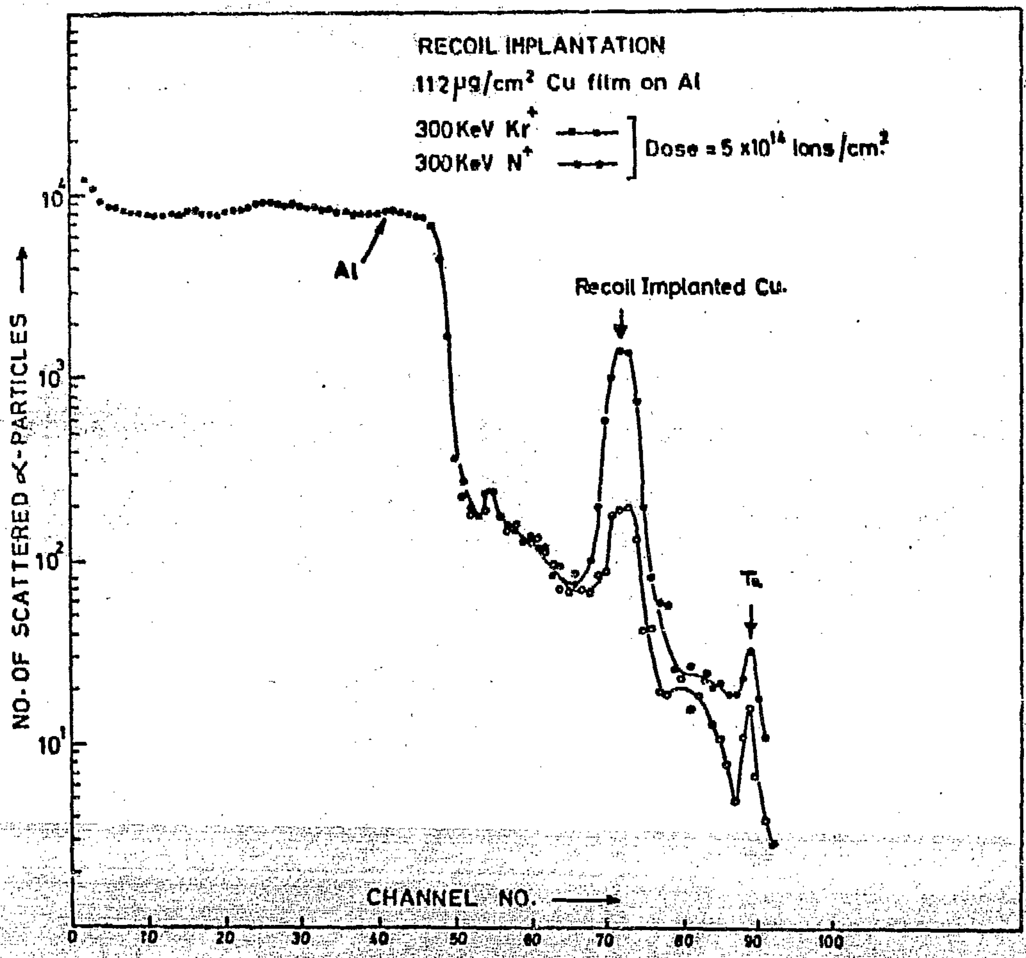
RECOIL IMPLANTATION
112 μg/cm² Cu film on Al
300 KeV Kr⁺
300 KeV N⁺
Dose = 5 x10¹⁴ Ions/cm²
Al
Recoil Implanted Cu.
Ta
NO. OF SCATTERED α-PARTICLES
CHANNEL NO.
0
10
20
30
40
50
60
70
80
90
100

FIG.20

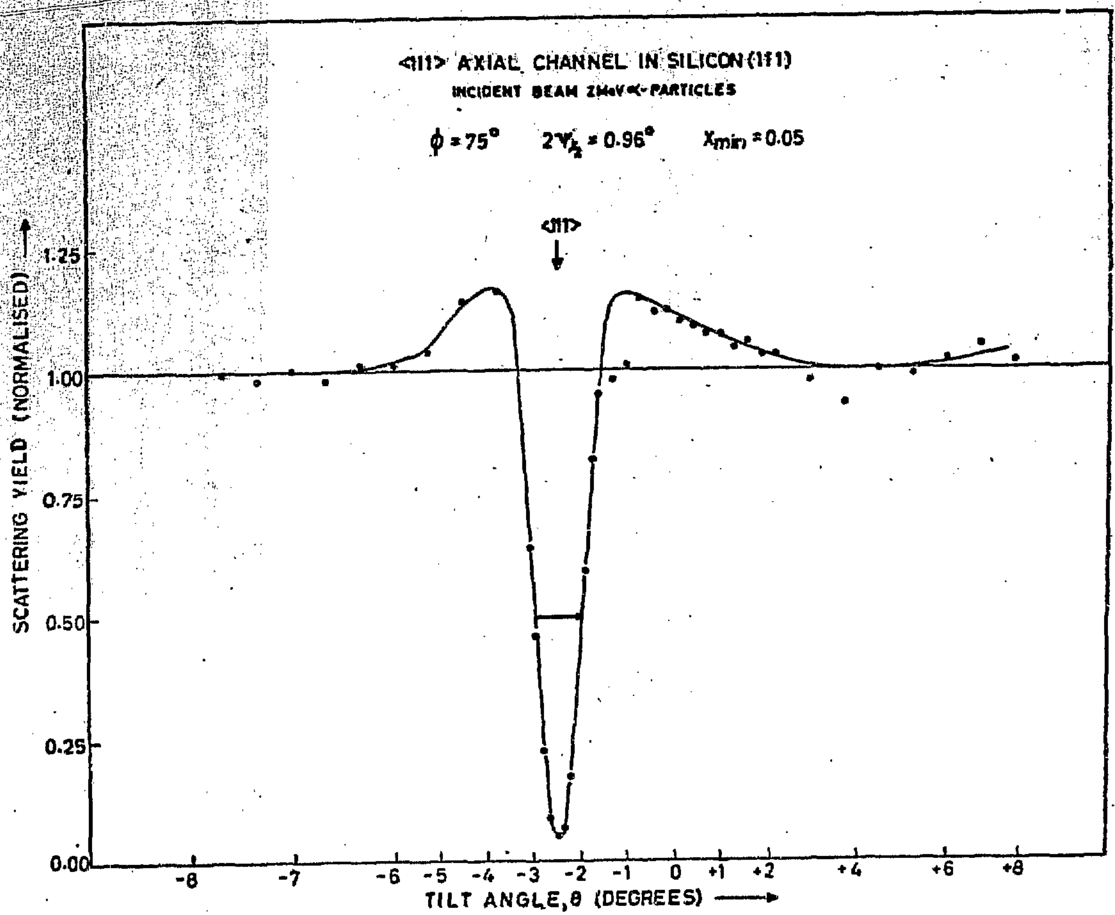
<111> AXIAL CHANNEL IN SILICON (111)
INCIDENT BEAM 2MeV α-PARTICLES
$\phi = 75°$
$2\Psi_{1/2} = 0.96°$
$X_{min} = 0.05$
<111>
SCATTERING YIELD (NORMALISED)
1.25
1.00
0.75
0.50
0.25
0.00
-8
-7
-6
-5
-4
-3
-2
-1
0
+1
+2
+4
+6
+8
TILT ANGLE, θ (DEGREES)

FIG. 21

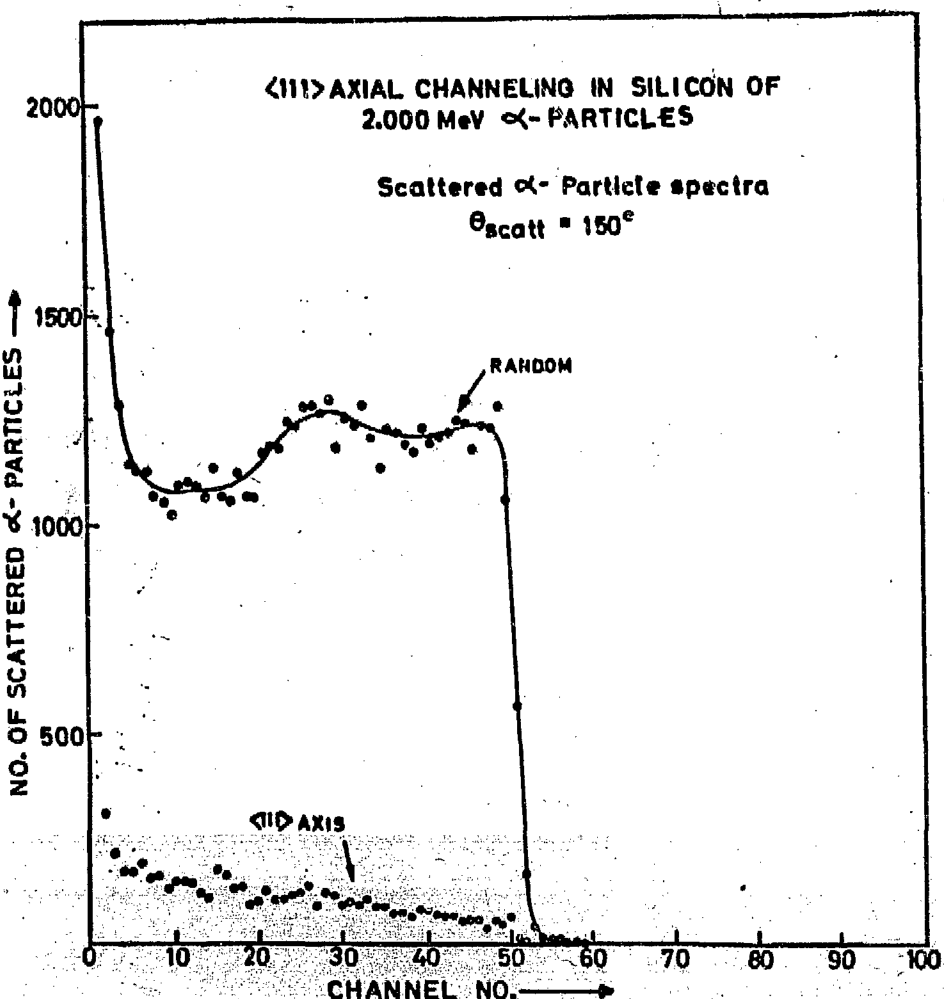

<111> AXIAL CHANNELING IN SILICON OF
2.000 MeV α- PARTICLES
Scattered α- Particle spectra
θ_{scatt} = 150°
RANDOM
<111> AXIS
NO. OF SCATTERED α- PARTICLES
CHANNEL NO.
2000
1500
1000
500
0
10
20
30
40
50
60
70
80
90
100

FIG. 22

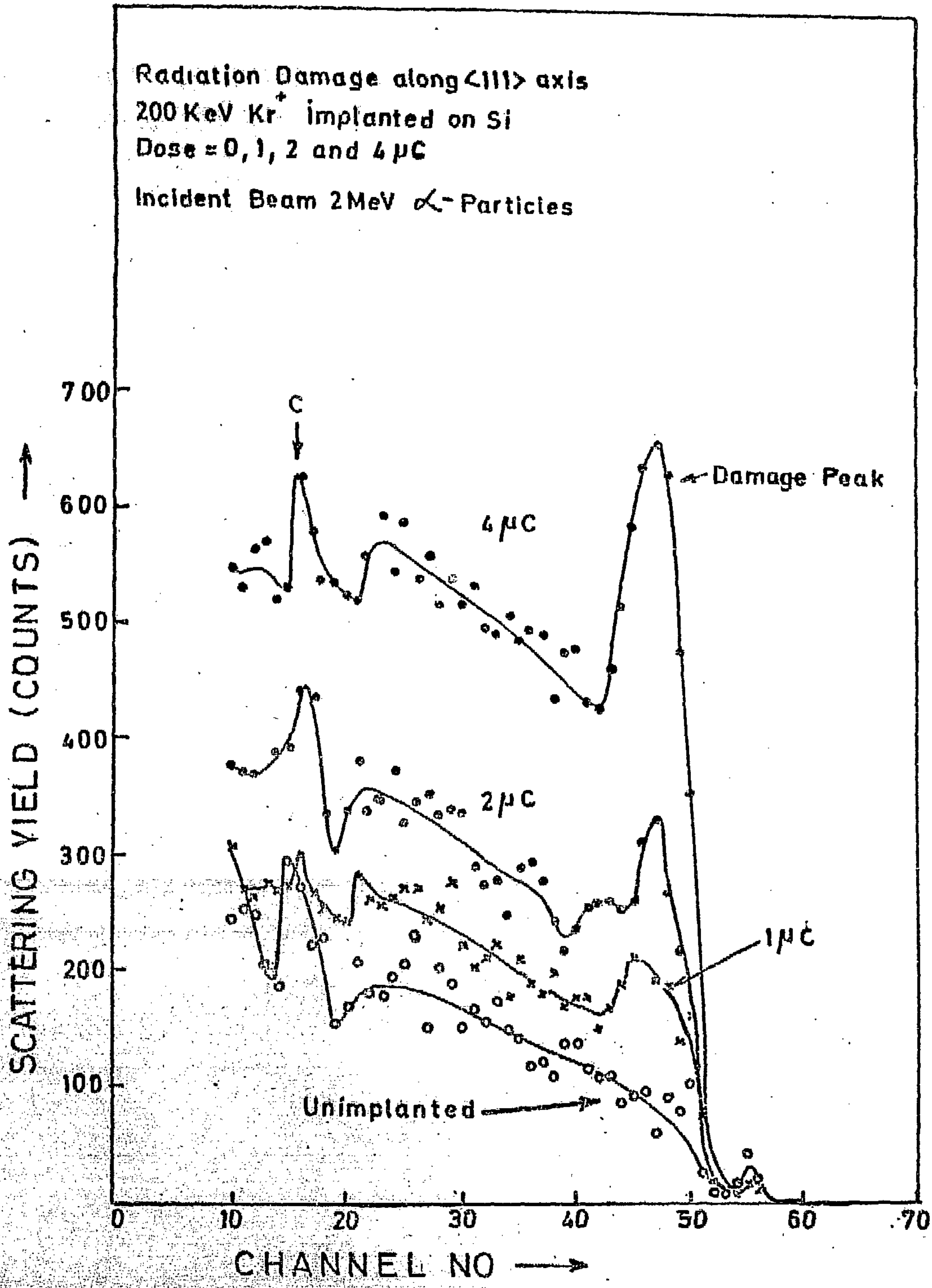

Radiation Damage along <111> axis
200 KeV Kr+ implanted on Si
Dose = 0, 1, 2 and 4 μC
Incident Beam 2 MeV α-Particles
C
Damage Peak
4 μC
2 μC
1 μC
Unimplanted
SCATTERING YIELD (COUNTS)
700
600
500
400
300
200
100
0
10
20
30
40
50
60
70
CHANNEL NO

FIG. 23